SciencePG
Science Publishing Group

Simulation and Analysis Method of Different Back Metals Contact of CH₃NH₃PbI₃ Perovskite Solar Cell Along with Electron Transport Layer TiO₂ Using MBMT-MAPLE/PLD

Ali Husainat[1, *], Warsame Ali[2], Penrose Cofie[2], John Attia[2], John Fuller[2], Abdalla Darwish[3]

[1]Department of Electrical and Computer Engineering, Prairie View A&M University, Prairie View, USA

[2]Department of Electrical and Computer Engineering, Faculty of Electrical Engineering, Prairie View A&M University, Prairie View, USA

[3]School of Science, Technology, Engineering and Mathematics (STEM), Faculty of Physics, Dillard University, New Orleans, LA, USA

Email address:
ahusainat1@student.pvamu.edu (A. Husainat), whali@pvamu.edu (W. Ali), pscofie@pvamu.edu (P. Cofie), joattia@pvamu.edu (J. Attia), jhfuller@pvamu.edu (J. Fuller), adarwish@dillard.edu (A. Darwish)

[*]Corresponding author

Abstract: Many different photovoltaic technologies are being developed for better solar energy conversion. Until now, crystalline Si solar cell represents the dominant photovoltaic technology with a market share of more than 94% with an efficiency between (15%-20%). Organic-inorganic halide Perovskite Solar Cell (PSC) has emerged as the most promising candidate for the next generation high-efficiency solar cell technology that attracted interest from researchers around the world due to their high efficiency of more than 24.% in a short period from (2008-2019) and low fabrication cost. In this paper, we designed a lead-based PSC model with a cell structure of Glass/FTO/TiO₂/CH₃NH₃PBI₃/Spiro-OMeTAD/(Au, Ag, Al, Cu, Cr, Cu-graphite alloy, and Pt) and analyzed the structure with different contact materials using Solar Cell Capacitance Simulator (SCAPS-1D) which is well adopted by many researchers to study and analyze the hybrid solar cell. Using the software allows researchers to inexpensively and promptly, the effect of the absorber and the contact materials on the performance of the proposed solar cell model. We also studied the bandgap of the active layer, defect density, thickness, operating temperature, and the fabrication method of the model. Furthermore, the adoption of multibeam multi-target MAPLE and PLD or with acronym MBMT-MAPLE/PLD techniques as a new fabrication method in our simulation program mentioned above. A promising result was achieved. Efficiencies of 27.25%, 26.52%, 18.90%, 25.66%, 22.77%, 27.25%, and 27.25% were obtained for the devices with Au, Ag, Al, Cu, Cr, Pt, and Cu-graphite alloy, respectively. The effect of the work function on the back contact has a significant influence over the FF and efficiency.

Keywords: Inorganic Materials Modeling, Organic Materials, Perovskite Solar Cell, Photovoltaics, Simulation, MAPLE, PLD

1. Introduction

The fastest developing renewable energy globally is solar-generated electricity, whereby the net solar generation is increasing by approximately 8.3% annually [1]. China has recorded the highest progression rates, followed closely by Japan and the USA, with the fourth to sixth positions being held by European nations, namely the United Kingdom (UK), Germany, and France in that order [2]. Ninety-eight percent of the current global market share consists of seven commercial technologies where the thin-film sector only contributes a meager 13% of the total. Nonetheless, the thin film industry growth rate surpasses that of the crystalline silicon industry [3-5]. The 13% market share is further demarcated into different established and emerging PV technologies such as amorphous silicon, dye sensitive, polycrystalline CdTe thin films, CIGS, quantum dots, as well as organic solar cells. Furthermore, to increase the market

share of this new type, a new approach has to offer an appropriate mix of reduced manufacturing costs, high conversion efficiency, as well as outstanding stability in different environmental conditions. Recently, the progress in hybrid organic-inorganic metal halide perovskite, methylammonium halide perovskite $CH_3NH_3MX_3$ or $MAMX_3$ (MA = CH_3NH_3, M = Pb or Sn, X = Cl, Br, and I) or merely perovskite, solar cells can potentially turn out to be among the foremost know-hows in PV business because of their high efficiency and reduced low fabrication costs. Due to exhaustive research measures worldwide for the past decade at the laboratory scale, the outstanding performance of perovskite-based solar cells is now equivalent to silicon-based solar cells [6-8]. German mineralogist Gustav Rose first discovered calcium titanate or calcium titanium oxide (CaTiO3) in 1839. The name of the mineral perovskite was named after Russian Mineralogist Lev A. Perovski (1792-1856) [9]. In hybrid organic-inorganic metal halide perovskite ($CH_3NH_3MX_3$), CH_3NH^+ features as an organic cation, M is a divalent metal cation (Pb^{2+} or Sn^{2+}), while X is a monovalent halide anion (Cl^{-1}, Br^{-1}, or I^{-1}). Due to their outstanding optoelectronic properties and potential solution-processed synthesis, these resources have been researched to constitute new resources for organic-based light-emitting diodes, as well as field-effect transistors (FET) [10-14].
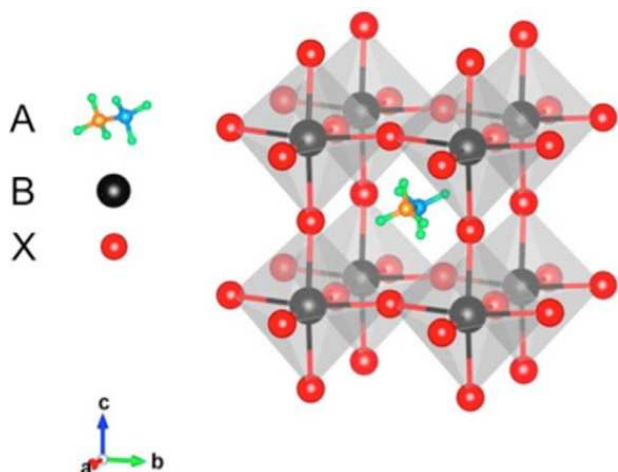
Figure 1. *Crystal structure of Hybrid organic-inorganic metal halide perovskite with chemical formula ABX₃ [1]*
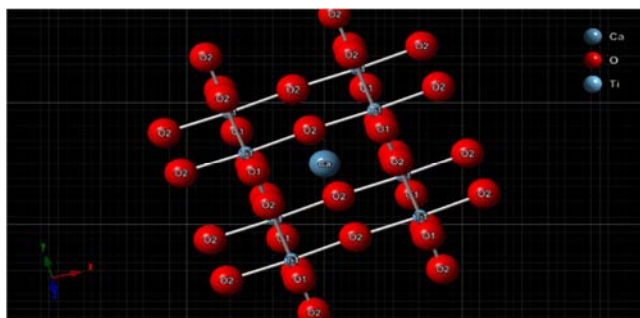
Figure 2. *Same as Figure 1, but different view: Many ABX₃ compounds adopt the perovskite structure, with A ions occupying large, 12-fold coordinated sites; B ions are in octahedral coordination by X [16].*
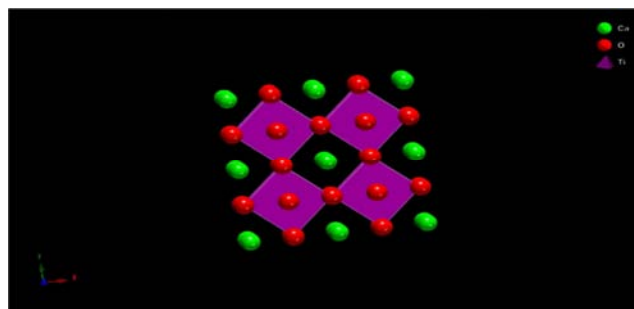
Figure 3. *CaTiO3 Perovskite - TETRAGONAL phase: each titanium atom bonds to six nearest-neighbor oxygen atoms [16].*

Any material that has a similar crystal structure to the mineral $CaTiO_3$ (Figure 1, Figure 2, and Figure 3) at a different transition state is called perovskite. The figures above depict a graphic illustration of the generic ABX_3 perovskite crystal configuration for a hybrid organic-inorganic halide perovskite [15]. The A position entails an organic citation ($CH_3NH_3^+$), B entails a metal citation (Pb^+ or Sn^+), and X being a halide anion (Cl^- or Br^- or I^-). The mixture of organic-inorganic lead halide perovskite composite was initially used in 2009 as visible-light sensitizers for photovoltaic cells with a 3.8% efficiency for X= Br and 3.1% for X=I, at one sun illumination [17]. In 2011, another role of perovskite entailed being a sensitizer in quantum dot sensitized solar cells, where it generated an efficiency rate of 6.5% [18]. These two performances portrayed the prospect of employing perovskite for solar cells despite their unstable nature, due to a liquid electrolyte presence. In 2012 an initial study was conducted, and the first solid-state perovskite solar cell was fabricated with a recorded efficiency of 9.7% [19], whereas another science publication report on solid-state perovskite solar cell, occurred in the same year with an efficacy of 10.9% [20]. The years after this era have recorded an increase in solar cell performance with 2015 marking the best efficiency mark of 22.1% [6]. The perovskite solar cell growth has depicted a remarkable trend within a diminished time and is deemed to be the most momentous scientific revolution in the PV industry [22-24]. Vapor-based and solution-based deposition are the two main deposition techniques employed in the construction of high-grade perovskite thin films. The deposition methodology that is based on solutions is not only cost-efficient but also attuned with the method of manufacture, which entails flexible substrates [25-27]. On the contrary, the deposition method that is vapor-based is an industrial production method with a prospect for the business-end of perovskite solar cells [28-29]. In either instance, the deposition techniques are comparatively quick and use minimal material quantity. This reason endears scientific communities towards the perovskite solar cells sector. The hybrid organic-inorganic metal halide perovskite-based material portrays various remarkable electrical and optical features that suit photovoltaic uses.

Perovskite's absorption coefficient of (alpha > 105 cm^{-1}) surpasses that of prevailing PV materials, for instance, GaAs, CIGS, CdTe, and Si with least Urbach energy and makes use of all the radiations more than the bandgap energy and offers

inflated short circuit current density (J$_{SC}$) beginning from ~300 nm thick films [30-31]. Methylammonium triiodide Urbach's energy is ~15 meV, nearing high-quality GaAa's Urbach energy [32]. Methylammonium lead tri-iodide's bandgap is estimated at 1.5 eV [33], and the incorporation of other halide ions within the range of 1.5 to 2.3 eV can aid in its tuning [34]. An extremely high open-circuit voltage (V$_{OC}$) is attained from perovskite solar cells compared to its bandgap as well as other thin-film solar cells [34-35]. A study by Wolf et al. [31], according to Eperon et al. (2014) [31], discovered extremely sharp concentration brink with insignificant deep defect states and slightest nonradiative rearrangement loss. There are three critical attributes possessed by perovskite materials, for instance, high hole and electron mobilities ranging from 10-60 cm2 V-1s−1 [36-38], long diffusion durations (>1 micro m); as well as long carrier lifetime reaching levels of 1.07 µs [39]. Additional studies by Chen et al. (2016) [40] established more long diffusion lengths and carrier lifetimes, reaching up to 30 µs and 23 µm for polycrystalline films and 3 ms and 650 µs for single crystals, respectively. All these variables account for the high Voc degrees characteristics of perovskite solar cells. Despite the high photo-conversion efficiency derived from perovskite solar cells, there is still a serious challenge regarding the solar cells' stability in ambient environments, and developments are quite slow and yet it is the main deterrent to their commercialization.

Due to the high volatility of the leading materials constituting perovskite solar cells, the organic species can not only leak from perovskite films and mix with humidity, but their ecological adaptability also reduces at merely somewhat elevated temperatures. For hybrid organic-inorganic solar cells, when conducting current-voltage calculations, the output depends on the way that bias current is applied to solar cells where it does not occur in normal inorganic solar cells, such as CIGS, Si, GaAs, and CIGS. [40-42]. Eventually, environmental worries surround the deployment of hazardous materials, for instance, perovskite and lead in perovskite solar cells.

Perovskite solar cell (PSC) has a high potential of leading thin-film technology as it shows a rapid efficiency increase in just a few years at laboratory level figure 10. Silicon-based solar cells have been dominating the solar market for many years with 94% market share, with an efficiency of only between 12%-17.5%, which led to an extensive search for new solar material for better efficiency. Hybrid organic-inorganic perovskite solar cells gained a lot of researchers' attention worldwide with a lab efficiency of 3.8% in 2009 to 24.00% in 2019 for single-junction solar cells. Perovskite material has a unique characteristic such as high absorption coefficient, high charge carrier mobility (i.e., 20cm^2 V^{-1}S^{-1}), long diffusion length for electron and hole, and a carrier lifetime. Perovskite solar cells offer a combination of low-cost lab fabrication and device performance [41-42]. Furthermore, perovskite solar cell has the optical and electrical property to absorb not only the visible light but also the NR as well, comparing to silicon solar cells which can absorb only the visible light spectrum. As of mid-2019,

perovskite solar cell lab efficiency has passed 24%, which makes it a promising better efficient cell to silicon. In this study, we have used a simulation program called SCAPS 1D (a Solar Cell Capacitance Simulator 1 D). In order to model a new fabrication method to the PSC layers, as shown in figure 17 called multi-beam multi-target matrix-assisted pulsed laser evaporation/ plus laser deposition or with the acronym (MBMT-MAPLE/PLD) that produces a uniform and fewer pinholes or defects in the absorber layer film, which decreases the carriers recombination mechanism. Figure 6 shows the solar device is a lead-based PSC model with a cell structure of Glass/FTO/TiO$_2$/CH$_3$NH$_3$PBI$_3$/Spiro-OMeTAD/ (Au, Ag, Al, Cu, Cr, Cu-graphite alloy, and Pt). To optimize the PSC for optimum efficiency, we must optimize the following parameters such as 1-Solvent to film optimization. 2-Band gap optimization. 3-Electron and hole transport material optimization. 4- deposition techniques that will be discussed later. We have also examined the effect of the absorber layer thickness, electron transport layer TiO$_2$, hole transport layer SPIRO-OMeTAD, work function of different back contacts, and the defect in the active layer on the overall performance of the perovskite solar cell, using Solar Cell Capacitance Simulator (SCAPS-1D) which is well adopted by many researchers to study and analyze the hybrid solar cell. Using the software allows researchers to inexpensively and promptly the effect of the absorber layer, defect density, and the contact materials on the performance of the proposed solar cell model. The optimum thickness of 500nm was concluded for the perovskite active layer for maximum efficiency. A promising result was achieved in table 1. In order to model the perovskite solar cell, we used real experiment data in the simulator to analyze the perovskite solar cell. Research work will continue to improve efficiency in terms of simulation and implementation.

2. Perovskite Structure

The structure of the hybrid organic-inorganic metal halide perovskite thin layer solar cell device closely resembles that of the dye-sensitized solar cell (DSSCs), only that it is a little bit modified [17-18]. The DSSC procedure involves the deposition of a porous TiO$_2$ film onto SnO2: F, which is then covered with dye particles and the structure immersed into a fluid electrolyte set in the metal conductor, for instance, platinum (Pt) [46]. For the metal conductor, a detached metal (Pt) plate is developed, encompassing a thin iodine electrolyte layer covering a conducting sheet. The pair of metallic pieces are then wrapped together to deter the leakage of the electrolyte. Kim et al. (2012) [19], manufactured the first solid-state perovskite solar cells by gathering MAPbI$_3$ onto sub-micron dense mesoporous TiO$_2$ film and finalized the solar cells by placing a hole-transport layer Spiro-OMeTAD and back contact metal, Au. This achievement preceded another manufacturing method by Lee et al. (2012) [20], whose efficacy was 9.7%. Apart from popularizing perovskite solar cells among scientific enthusiasts, the two fetes have also attained a couple of indicators within the

sphere of device execution using mesoporous structures [23, 43-45]. Also, to fabricate mesoporous solar cells TiO$_2$ films, a high annealing temperature is required, which could not only be costly but also time and energy consuming. As previously stated, that MAPbX$_3$ possesses a comparatively long charge carrier diffusion length which indicates that both holes and electrons can easily be transported to their respective contacts without the need of addition TiO$_2$ mesoporous layer, which cut on the fabrication time and cost as well [43]. Hence, rather than being restricted to mesoporous configurations, researchers began to focus on planar device structures where the perovskite thin film is placed onto a compressed electron transport layer (ETL) as opposed to a mesoporous layer. Through a dual-source vapor layering procedure, planar perovskite configurations managed to attain an efficiency rate of 15.4% in 2013; the current uppermost productivity derived from this form of structure is approximately 20% [25-26]. In both forms of device configurations, there is a possibility of illuminating solar cells through either the ETL layer to generate an n-i-p structure or the hole transport layer (HTL) to produce a p-i-n structure or inverted. Perovskite material is a direct bandgap between 1.3ev and 2.2 eV, which gives it the optical property to harvest and convert near-infrared (NIR) and ultraviolet (UV) light into visible light, which can be utilized by the perovskite active layer as shown in figure 4 [46-48]
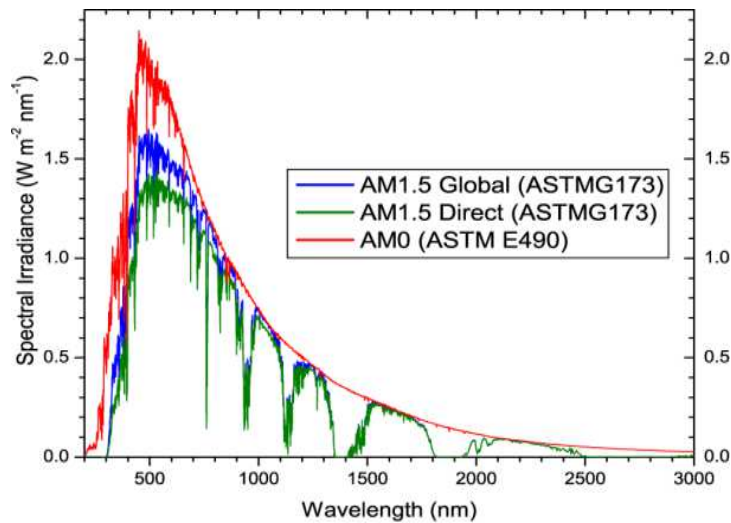

Figure 4. *Standard solar spectral (source PVeducation.com).*

In the 1990s, scientists discovered that halide perovskite could convert light into electricity. Due to this discovery, the light-emitting diodes (LED) were made. Perovskite structure has four possible phases, such as 1) α is cubic structure phase accrue at T > 327 K. 2) β is a tetragonal structure phase accrue at T< 327° K, 3) γ is orthorhombic structure phase accrue at T=160° K. 4) δ is a polyhedral phase structure which is a none perovskite phase [49-50].
The tolerance factor giving by equation (1):

In order to maintain the cubic structure of the perovskite layer, the tolerance factor should be close to one, where R$_A$, R$_B$, and R$_X$ are the radius of the ions. In order to have a stable perovskite, the tolerance factor must be in the range of 0.7< T < 1, which maintains and hold the bond between both cations. Cation A >> cation B to have a stable perovskite structure. Therefore, Methylammonium (MA+) ion is one of the best organic material options. The transformation of perovskite depends on the tilting and rotation of BX$_6$ [47-49].

$$t = \frac{(R_A + R_X)}{\sqrt{2}\,(R_B + R_X)} \qquad (1)$$

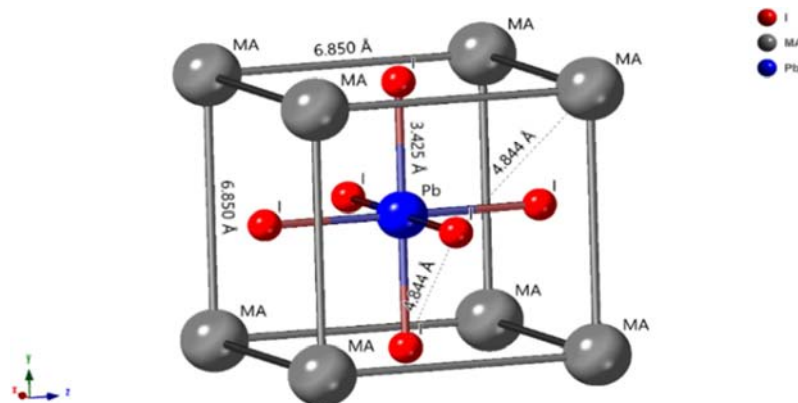**Figure 5.** *Cubic structure of MAPbI$_3$ with symmetrical distant between MA-MA, Pb-I atoms [16].*

This comparison makes the perovskite a promising candidate. The primary goal of designing a highly efficient solar cell is to optimize the power conversion efficiency (PCE) to cost ratio. Furthermore, and due to this rapid research and improvement of the perovskite family, MAPbBr₃, MAPbCl₃, and MAPbI₃ Methylammonium lead iodide (MAPbI₃) is the one that proved to be the best perovskite material due to its excellent electrical and optical properties, low-temperature solution processability, long lifetime, and ferroelectricity. The efficiency of the perovskite solar cell can be further improved through different design techniques to not only the absorber layer but to all other six layers, as shown in Figure 6 [16].

Figure 7 shows the energy levels of the device Layers; it must be in this position for a smooth transfer of the electrons and holes through their transport layers to the electrodes.
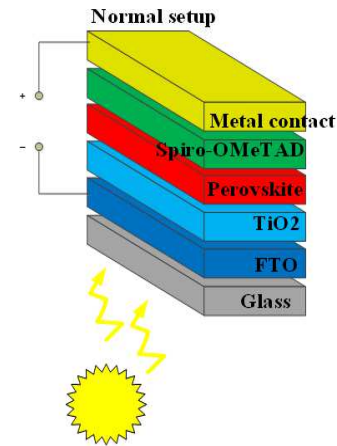

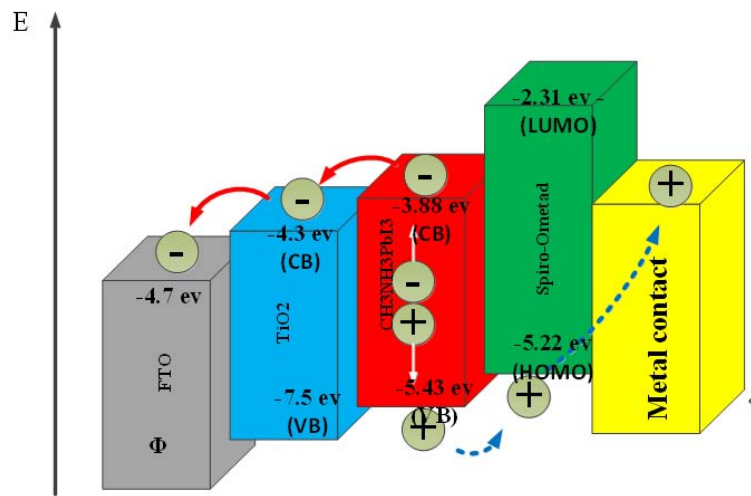**Figure 6.** *Perovskite solar cell normal setup [16].*

Figure 7. *Energy Levels of the Device Layers [16].*

2.1. Mesoporous Scaffold Structure

There are two classes of these structures based on the angle of incidence of the light on the solar cells. The pioneering employment of perovskite solar cells was dependent on mesoporous n-i-p configuration, and to-date is still extensively employed to manufacture high achievement solar cells. Within the mesoporous n-i-p configuration, a sheet of approximately 50-70nm thick solid ETL (TiO₂) is placed on the tin oxide (FTO: SnO₂: F) doped with fluorine and coated glass substrate. A 150-300 nm thick mesoporous metal oxide (TiO₂ or Al₂O₃) occupied with perovskite covers the ETL. Approximately 300 nm perovskite is progressively placed before the placement of a 150-200 nm HTL (Spiro-OMeTAD) and back contact metal (Au). An overturned p-i-n mesoporous construction in perovskite solar cells can similarly be attained [51]. A typical device configuration of mesoporous inverted p-i-n is made up of the following arrangement, FTO/compact NiOx/nanocrystal NiO/perovskite/PCBM/ electrode. Within the mesoporous n-i-p construction, electron transference between mesoporous and comparative conductive TiO₂ or insulating Al₂O₃

scaffolds is employed to enable electron transport amid the perovskite absorber as well as the FTO conductor [36]. A widespread hole-blocking in the mesoporous construction is critical to (1) prevent the current leakage between two contacts, (2) increase the photon absorption because of light scattering, and (3) improve the carriers' collection [52]. For optimum light absorption and maximizing carrier's generation, there is a need to reduce the resistance and increase the shunting pathways by adding a perovskite covering coating that is usually preferred on top of the mesoporous construction. Also, in case of a mesoporous configuration that is denser, the perovskite resources restrained within the openings lack enough space for adequate grain development, therefore eventually reducing the device performance and dropping the V_{OC} and J_{SC} [53-54]. Hence, the mesoporous TiO₂'s thickness not only defines the hole filling portion and perovskite particles but also establishes the current conveyance rate as well as the collection efficiency at the interface of perovskite/TiO₂. The cross-section picture and illustrating the current-density-voltage (J-V) features of a typical mesoporous configuration are shown below, together with corresponding J-V

parameters 59 [54].
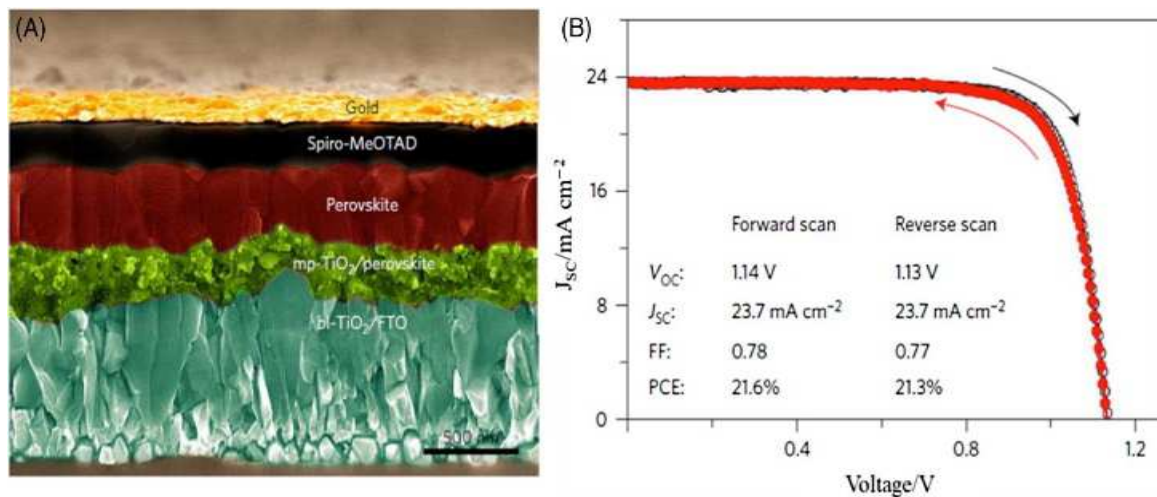
Figure 8. *(A) a colored picture of scanning electron microscope (SEM) perovskite solar cell using a polymer-templated nucleation and growth (PTNG) method, (B) J-V curve of the perovskite solar cell prepared by PTNG method 59 [54-55].*

2.2. Planar Structure

The mesoporous scaffold layer in the planar construction of perovskite solar cells is removed, and only the perovskite absorber layer is sandwiched between the HTL and ETL. The planar configuration is considered an evolution of the mesoporous device structure. The simplicity of the new planar device structure of perovskite solar cells has fascinated researchers within the field of thin-film PV cells. Within the n-i-p planar configuration, the ETL side is used to illuminate the solar cell while in the p-i-n planar construction, illumination from the HTL side. The initial positive demonstration of planar configuration had a minimal efficacy of 4% because of the inferior film superiority and insufficient photon absorption of the perovskite film 60 [56]. Currently, the planar construction depicts an efficiency performance that resembles the mesoporous structure. The original solar cell configuration in both instances is made up of glass/ TCO /ETL /perovskite / HTL /metal and glass /TCO /HTL /perovskite /ETL /metal, respectively [56-57]. There has been a heightened efficiency associated with planar n-i-p solar cells with emerging progress that have driven the current efficiency to 19% [58]. The perovskite solar cell's J-V curves lack congruence when scanned from front to back and back to front contrasting with other normal solar cells, for instance, CGTS, CdTe, and Si. The n-i-p planar structure figure (9B) portrays more of this characteristic. The inverted p-i-n planar figure (9C) configuration is similar in characteristics to organic solar cells. The classic organic-based transport films, for instance, [poly(3,4-ethylene dioxythiophene) polystyrene sulfonate] (PEDOT: PSS) and fullerene derivative [[6,6]-phenyl-C61-butyric acid methyl ester (PCBM)] are directly applied similar to ETL and HTL sheets of perovskite solar cells. Likewise, rather than employing the FTO substrate, the p-i-n construct prefers the indium oxide doped with a tin (ITO) substrate. The enhanced choice of fullerene derivatives has immensely enhanced the efficacy of the p-i-n planar construct from an initial 3.9% to the current 18.9% [59-61]. The typically used HTLs in the p-i-n configuration entails PEDOT: PSS, PTAA (poly-triarylamine), and NiOx and ETLs are PCBM, PC61BM, C60, ZnO, as well as their blends [62-65]. The current-density voltage features with J-V limits and external quantum efficiency (EQE) information of perovskite solar cells in a planar structure are shown in figure 9 [66].
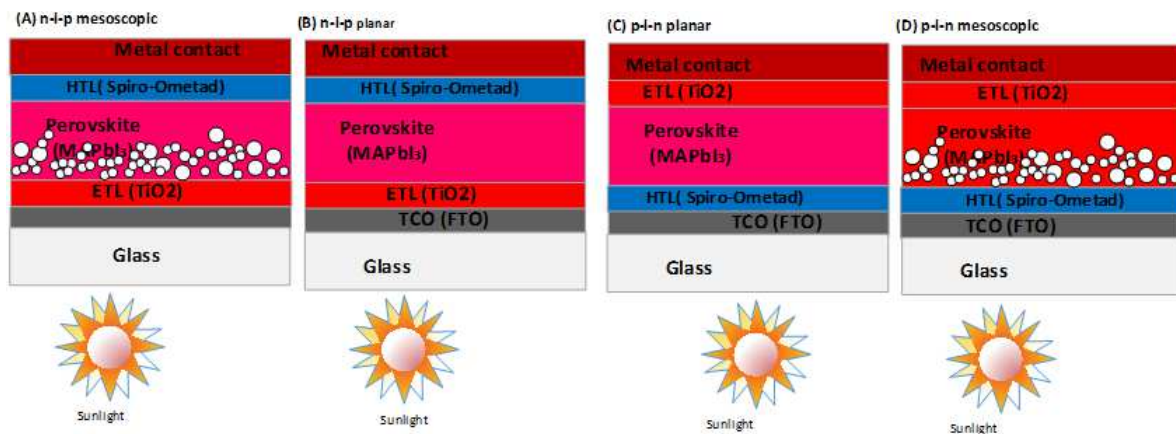
Figure 9. *Schematic diagram of perovskite solar cell in the (A) n-i-p mesoporous, (B) n-i-p planar, (C) p-i-n planar, and (D) p-i-n mesoporous structures [16].*

3. Device Optimization

The development of solar cell device optimization is an ongoing process, and in order to make an efficient solar cell, each layer needs to be optimized. Since some of the layers in the perovskite solar are already well studied and optimized, emphasize has been focused on developing the technology of fabricating the thin film of three main layers ETL, the perovskite absorber layer, and HTL. Figure 10 shows an upsurge in solar efficiency from 3.8% to above 24.1% in the past nine years alone is majorly attributed to the creation of the n-i-p mesoporous configuration due to world research efforts, comparing to other thin-film technologies, particularly and silicon solar cells in general. In the case of optimizing the absorber layer,
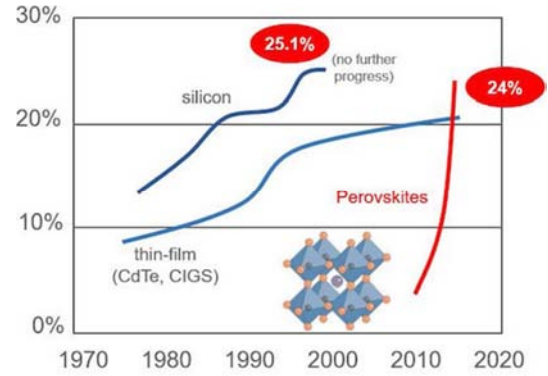
Figure 10. *Comparison of the lab efficiencies of Silicon, thin-film, and Perovskite over the years. Source: International Tin Research Institute.*
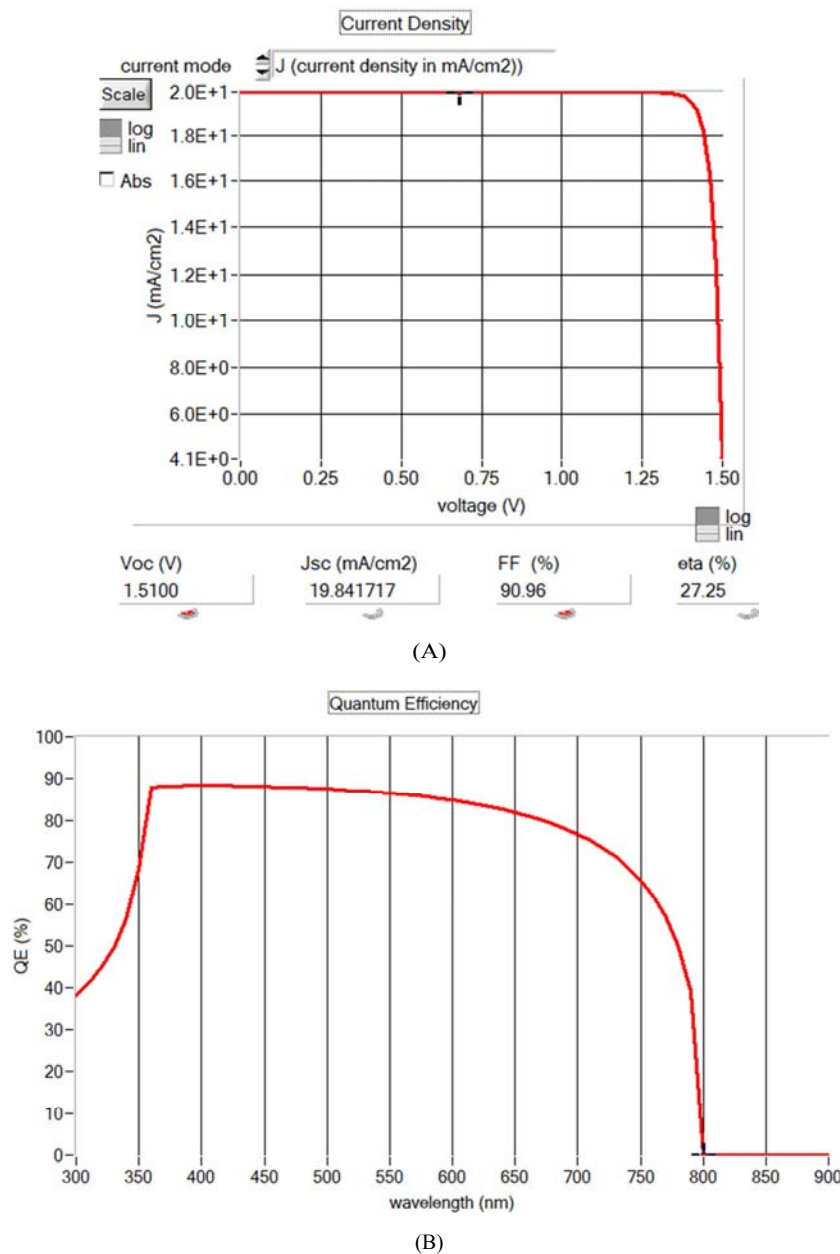
Figure 11. *(A) The J-V characteristics perovskite solar cells in a planar device structure under 1-sun illumination figure 6, (B) EQE of the solar cell with the active layer of CH₃NH₃PBI₃.*

The focus is on selecting the appropriate precursor solution and the processing methods of making a thin film to obtaining smooth, pin-hole free perovskite films consist of large grains with good crystallinity and the interference with other layers free of a defect to minimize the recombination effects. The following optimization has achieved by using the SCAPS 1D simulator based on the MBMT-MAPLE/PLD method of making ETL, perovskite absorber, and HTL thin films a smooth and pin-hole free with a minimum defect. Figure 11(A) shows an efficiency of 27.25% reached, with a Voc and Jsc of 1.51V and 19.841717 mA/cm^2 respectively, and external quantum efficiency (EQE) as shown in figure 11(B) using Au as a contact layer, other contact layers were used also, and the results were obtained and listed in table 1. Device optimization is a vital process in the development of these solar cells in the quest for effective performance, and every layer ought to be optimized. Specific importance is, nonetheless, directed towards optimization of the key films, namely the substrate, ETL, HTL, as well as perovskite absorber layer and the contacts. Furthermore, it has attained an efficiency of above 24.1% within a very brief duration, quite a remarkable increase when equated to the advancement attained within other thin-film technologies. Regarding the utilization of the absorber film, the emphasis has been on regulating the precursor solution, the composition of perovskite, film processing, and solution dispensation, as well as the interface, features with the ultimate goal of attaining even, pin-hole free perovskite layers made up of large grains with desirable crystallinity. The below optimization was undertaken to enhance the perovskite solar cells' absorber layer.

3.1. Solvent to Film Optimization

The solvent engineering approach to the use of blended solvents or/and anti-solvent is an efficient but simple method for achieving satisfactory perovskite film morphology in the pursuit of high-perovskite solar cells [67-68]. The perovskite film manufacturing process involves the preparation of a precursor solution by liquefying it in a mixture of dimethyl sulfoxide (DMSO) and γ-butyrolactone (GBL) and spin coating using one or two-step methods. Among the widely used solvents, DMSO is used for the manufacture of metal-halide multiplexes owing to its reliable coordination with MX2. Kim et al. (2014) [69] also used a mixture of N, N-dimethylformamide (DMF), and GBL to produce a perovskite layer with enhanced layer superiority. In the making of films, anti-solvents, for example, toluene is used for removing excess solvents, e.g., DMSO and DMF for a fast sleeve of the perovskite substrate until substantial growth occurs [70]. The application of toluene to the film manufacturing process produces small-particle and dense perovskite films. The fast-deposition crystallization (FDC) process was demonstrated by Xiao et al. (2014) [71] to produce extremely even perovskite film using the MAPbI$_3$ DMF spin-coating solution and instantaneously accompanied by the aggregation of chlorobenzene to cause crystallization. This technique involves the accelerated solubility reduction of MAPbI$_3$ with fast nucleation and growth arising from the introduction of the second solvent [72]. The FDC-manufactured film produces a large grain and maximum surface exposure relative to partial exposure by conventional spin coating. A new notion of solution-solution separation was proposed for the processing of high-grade perovskite films at room temperature [73]. This technique involves a spin-coating perovskite surface in a solution with a vigorous boiling point, such as N-methyl-2-pyrrolidone (NMP), accompanied by an immediate transition of the wet film to low boiling point solvents such as diethyl ether for the crystallization of even perovskite films. Xylene and benzene are other anti-solvents used in the processing of high-grade film; the diagram below demonstrates the structural and morphological description of MAPbI$_3$ films collected from different deposition processes.

The post-deposition annealing technique is crucial in removing the residual solvent from the solution-process, in aiding the formation of perovskites from its precursor and in improving the production and crystallization of the sample. The combined halide perovskite, such as MAPbI3−xClx, needs to be hardened longer to achieve complete alteration, unlike single halide mode. There is a decline in surface treatment of perovskite film with an increase in annealing time (for example, over 30 min at 110 ° C) at an increase in temperature due to the degradation of the perovskite phase annealing at high temperatures (more than 80 ° C) usually ends in the loss of MAI and inflates the relative PbI2 content, resulting in a decline in device performance (de Quilettes et al., 2015) [75]. Typically, annealing happens either in dry air or inert atmosphere, such as in a nitrogen atmosphere. Perovskite films can also be annealed in MAI vapor or pyridine with a lifetime achievement and increased luminescence [76] (Tosun & Hillhouse, 2015). Likewise, Xiao et al. (2014) [77] conducted solvent annealing with DMF achieving enhanced perovskite layer crystallinity and progress in performance. The annealing of the perovskite layers is called hotplate annealing in different environments. Similarly, visual annealing tactics have been recorded for perovskite layers using either xenon light (intense pulse and photonic flashlight) or halogen lamp (near-infrared radiation) sources [78-80]. The optical annealing technique is known to be effective since the heat light/radiation is captured by the absorber layer in comparison to the FTO material. Nevertheless, it has been developed that the power conversion efficiency of perovskite solar cells does not agree with hot plate annealing procedures. The explanation behind this may be that it is almost impossible to measure temperature accurately in optical annealing procedures. The concept of "flash" annealing introduced by Saliba et al. (2014) [81] was primarily applied to planar architecture solar cells, where the sample annealed at high to low temperatures at various times intervals.
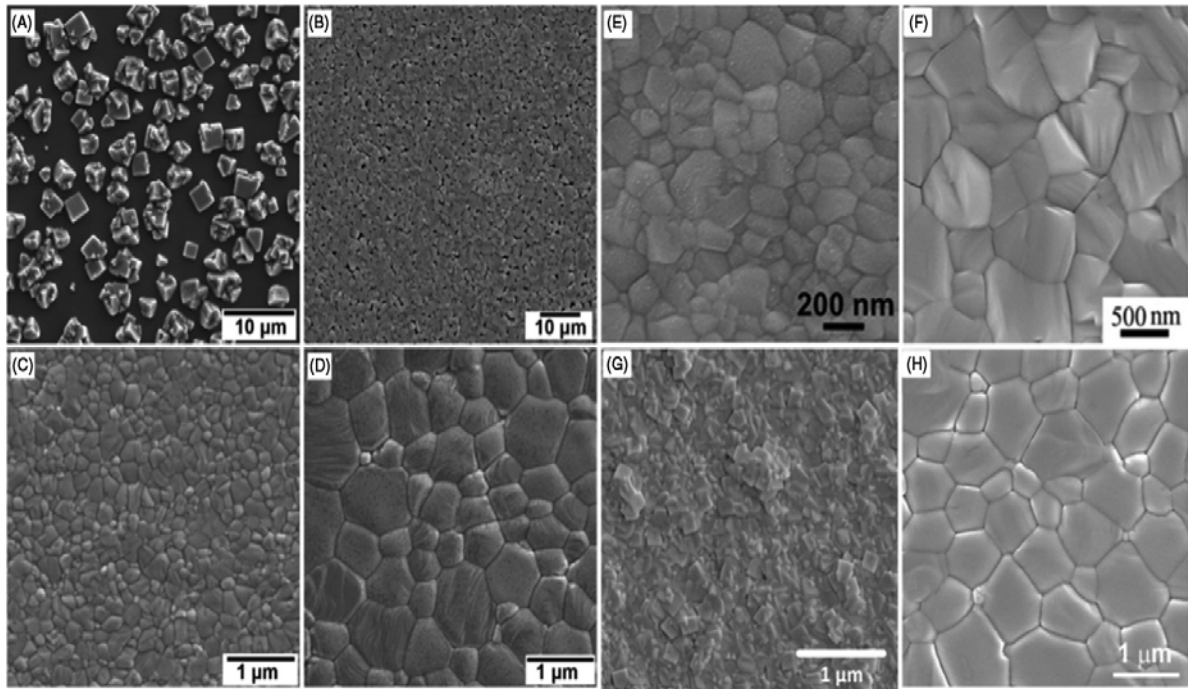
Figure 12. *Morphology regulation of hybrid organic-inorganic metal halide perovskite material: SEM images of CH$_3$NH$_3$PbI$_3$ developed from (A) one-step spin coating, (B) two-step spin coating, (C) one-step spin coating with toluene treatment, (D) toluene-treated film thermal annealing [83], (E) solvent-solvent extraction technique [72], (F) vapor-assisted deposition technique [26], (G) vapor deposition technique [27], (H) fast deposition crystallization method [74].*

3.2. Band Gap Optimization

It has been established that chemical modification of the anions organic-inorganic metal halide perovskite can tune the bandgap over a wide range of the solar spectrum. For instance, the bandgap of the perovskite can be chemically tuned to cover nearly the whole invisible solar spectrum from 1.5eV for MAPbI$_3$ to 2.3eV for MAPb(BrxI1−x)3 when x = 1, with a unique variation in photo-conversion efficiency (PCE) of perovskite solar cells [82]. Apart from tuning the bandgap of the material, the inception of Br also increases the stability of the material in a humid environment (Koh et al., 2014) [83]. The cation's alteration of perovskite's bandgap can also be tuned through the switching of Methylammonium with a formamidinium ion (FA) to develop formamidinium lead halide [(HC(NH$_2$)2PbI$_3$] perovskite configuration having to possess a bandgap of the perovskite [84-85]. Pellet et al. (2014) formulated an alloy of MAxFA$_1$−xPbI$_3$ to advance the absorption to an extended spectral range as well as improve the thermal stability. In the same light, Yang et al. (2015) [6] manufactured high efficacy solar cells by employing intramolecular interchange with the absorber: (MAPbBr$_3$)x(FAPb$_3$)1−x.

3.3. Electron and Hole Transporting materials Optimization

Perovskite / HTL and perovskite / ETL interfaces provide efficient charge separation for external electrodes. Appropriate HTL and ETL materials maintain a low surface and boundary load recombination that represents a high level of load quality. The most common metal oxide ETL need for high-performance perovskite solar cells is made up of mesoporous and planar TiO$_2$. The speeds the charge transmits to TiO$_2$ ETL film from the perovskite absorber layer are high. Likewise, due to the low transport and mobility properties, TiO$_2$ has strong recombination levels for electrons [86]. As ETL films in perovskite solar cells, nanorods, zinc oxide (ZnO), as well as nanoparticles resulted in productivities as high as 15.9 percent and 11.1 percent [87-88]. Mesoporous ETL layers have also used other metal oxides in perovskite solar cells, such as Al$_2$O$_3$, SiO$_2$, ZrO$_2$, and SrTiO$_3$ [89-91]. In planar architecture, zinc oxide was used as a thick ETL coating with an effectiveness of 15.7% [92]. Baena et al. (2014) [93] used SnO$_2$ as an ETL and fabricated highly efficient planar perovskite solar cell with an efficiency of 18 percent A planar n-i-p device layout involves other largely inorganic ETL materials such as TiO$_2$-graphene, CdS, and CdSe [94, 95, 96]. ETLs in solar perovskite cells often use products from ETL organic solar cells. Despite the admirable transport characteristics of organic HTL materials, they lack stability, unlike inorganic HTL materials, which have long-term stability and are also cost-effective, but their shortcomings are their low efficiency compared to organic HTLs. Inorganic HTL products contain Cu: NiOx, CuSCN, NiO, CuO, and the pyrite of iron, which called iron sulfide (FeS$_2$) [97-98].

4. Deposition Techniques

The output of the perovskite solar cells or other solar cells is judged primarily on the consistency of the film layer, given the significance of other layers. Several factors determine the manufacture of high-quality film and high-performance solar

cells, such as regulated morphology, thickness uniformity, high surface coverage with no or limited pinholes, substrate phase purity, and high crystallinity. For example, the high crystallinity of the film defines the efficiency of the carriers' separation, the charge transport, and the duration of diffusion of the load carrier [99-100]. In order to establish these requirements, the content structure engineering, the film processing process, the crystallization control, the required substrate selection, and the selection of solvents/additives are carefully performed. The essence of the surface morphology of the ground defines the consistency of the film produced on it. Perovskite film is of high quality when the substrates of concern are mesoporous, regardless of TiO_2, Al_2O_3, or NiO, and provides excellent system performance [101]. The crystal size of the mixed halide perovskite (MAPbI$_3$−xCl$_x$) is reduced to < 100 nm in the mesoporous Al_2O_3 relative to about 500 nm in the planar form, resulting in an increase in the JSC of the solar cells [102]. Various techniques for deposition of high-quality perovskite thin films are used, such as single-step solution deposition [20], two-step solution deposition [24], two-step vapor-assisted deposition [26] and thermal vapor deposition [27].

4.1. Single-Step Deposition

The organic and inorganic compounds are co-deposited either via thermal or solvent evaporation procedures [103-105]. The one-step solution procedure entails dissolving a blend of MX_2 (M = Pb or Sn and X = I, Br, and Cl) and Methylammonium iodide (MAI) or formamidinium iodide (FAI) in a carbon-based solvent and the solution combination is spun coated onto the relevant substrate. The resultant film is annealed at 100–150°C to generate the final perovskite phase. The composition variation involved in the deposition procedure employed in manufacturing high-performance solar cells is derived from MAI poor to MAI rich in PbI2 in the ratio of 1:23:1 [106-107]. The modified precursor composition would need to maintain the required phase purity, crystal structure, and morphology throughout modification in processing time and temperature [108-109].

4.2. Two-Step Sequential deposition

The formula entails the spin covering of an MX_2 seed layer onto the substrate, which is then immersed into MAI or FAI/isopropanol solvent, or an additional spin coating is prepared for FAI or MAI onto an MX_2 grid to develop a hybrid organic-inorganic metal halide perovskite film [24, 110]. The superiority of the two-step procedure is derived from the fact that it offers a more uniform and regulated film and has been widely employed in solar cell manufacturers [6, 24, 101]. Furthermore, there are some problems in the two-step process, such as incomplete perovskite conversion and surface roughness in some cases, although the concerns have been greatly simplified with the introduction of new technologies [103].

4.3. Two-Step Vapor Assisted deposition

This technique has been revised by Chen et al. (2013) [26], who described it as the MX_2 layer through a vapor deposition method to better regulate the grain size and morphology of the perovskite film. Further, there is a disadvantage to using this deposition technique. First, it takes a long time to make the perovskite thin film, and second, the performance of the film is not efficient due to then one- uniformity of the perovskite thin film.
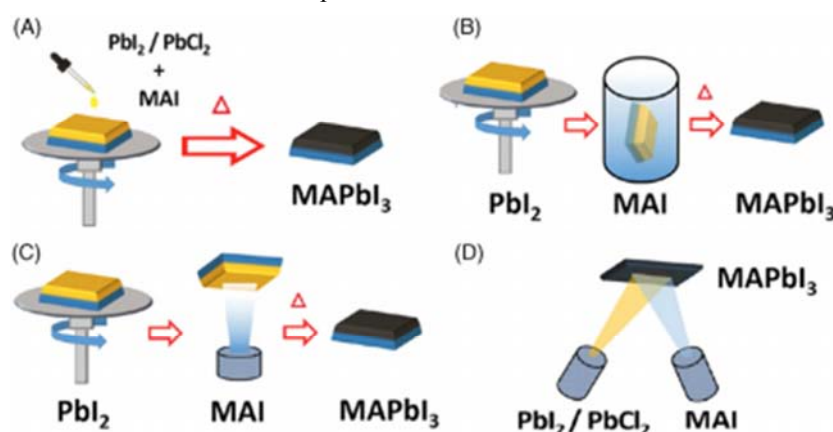
Figure 13. *Deposition methods for perovskite thin films, including (A) single-step solution deposition, (B) two-step solution deposition, (C) two-step hybrid deposition, and (D) thermal vapor deposition [103]*

4.4. Thermal Vapor deposition

This technique employs a dual source for MX_2 and MAI/ FAI with various heating components to establish perovskite layers [28]. This technique offers a high-grade perovskite thin layer with a uniform thickness and of pin-hole-free film. The initial planar heterojunction MAPbI$_3$−xCl$_x$ solar cell was manufactured in 2013 using a thermal vapor deposition process whose efficiency was >15% [27]. Among the main shortfalls of this method is the prerequisite of precise temperature control in the course of deposition since both precursor sources and the resultant film have low thermal stability.

4.5. PLD Method

The discovery of the first laser by Maiman in 1960 set the stage for laser-assisted film. Also, the utilization of the ruby laser by Smith and Turner in 1965 set the stage for the entire process. Breech and Cross studied the excitation of atoms and laser vaporization to deliver more quality films. The main breakthrough then came in the 1980s when the laser technology was ascertained by researchers, thus affirming the quality of films deposited. Since then, pulsed laser deposition techniques have been used widely in the creation of high-quality crystalline films. Pulsed laser deposition is a comprehensive blueprint that involves a high-power laser beam being concentrated in a vacuum to strike a material that is deposited [111]. PLD is also called a physical vapor deposition (PVD) technique. Consequently, the material is vaporized, thus becoming a thin film that is deposited on a substrate, for example, fluorine-doped tin oxide (FTO) facing the target. However, the process can only take place where there is a background gas, for instance, oxygen needed in depositing oxides [112]. Also, the process can operate in an ultra-high vacuum because it avails the right conditions for the thin films to be deposited. Film growth and laser-target interaction involve complex processes, which will be highlighted as the text progresses. First and foremost, the laser pulse is absorbed by the target, and then the remaining energy is converted. The energy is converted to electronic excitation and then into mechanical, thermal, and chemical energy, which leads to evaporation, ablation, plasma formation, and exfoliation. Finally, the ejected species expand in the form of the plume to the surrounding vacuum while containing many energetic species such as atoms, molecules, electrons, ions clusters, particulates, and molten globules. Therefore, the discussion will break down the pulsed laser deposition process into four main stages, which will be explained at length in the paper.
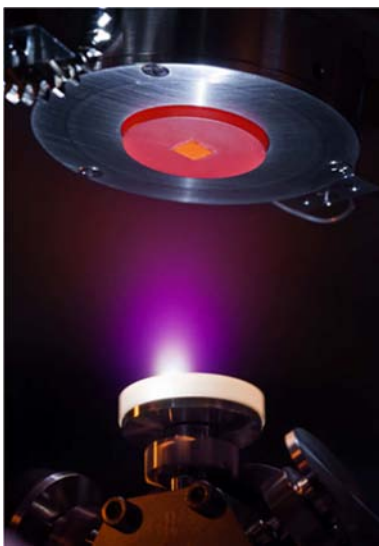

Figure 14. *Pulsed Laser Deposition chamber [120].*

Figure 14 shows a plus laser deposition of aluminum oxide (Al₂O₃) target sets on a white rotating disk to grow a thin film of aluminum oxide on strontium titanate (SrTiO₃) substrate which is glowing red due to the hot plate of 650C that sets to crystalline the desired film. This how we build up one atomic layer at a time, such as perovskite solar cell, which consists of 6 layers.
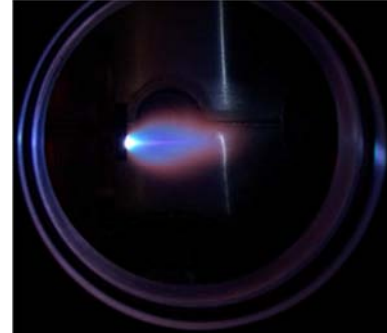

Figure 15. *Plasma plume of Al₂O₃ target material [120].*

Figure 15 shows a plasma plume it is an extension to figure 14, as you can see from the picture a purple plasm plume ejected from SruO₃ target, which the result of the laser pulse interaction with Al₂O₃ and the result is a visible purple cloud or mist will be deposited on the SrTiO₃ substrate to create alumina thin film

(A) The Process

The process of pulsed laser deposition mainly contains four main stages, as follows. One, there is laser absorption and ablation of the target material. Two, there is the creation of the plasma and the dynamic of the plasma. Three, the ablated material is deposited on a hot substrate, and finally, the film grows on the substrate surface. Each of these measures is critical to the crystallinity, uniformity, and stoichiometry of the desired thin film. Also, there are Monte Carlo techniques that are widely used in modeling the PLD process.
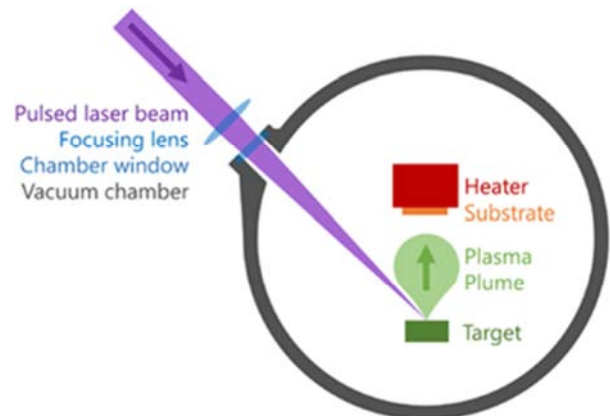
Figure 16. *Configuration of a PLD chamber, as seen in figure 14 [120].*

(B) Creation of plasma and Laser ablation

The process of laser ablation starts from the vaporizations, and removal of the bulk material from the surface region is considered a complicated process. Also, the process must consider the index of refraction and the laser wavelength of the target material, which is usually 10 nm. The laser light generates a strong electric field, which effectively removes

electrons from the bulk material. Then free electrons move aggressively in the electromagnetic field until they collide with atoms of the bulk material. Eventually, they transfer some of their energy to the lattice of the target material within the surface, after the collision the surface of the target heated up and start vaporizing which called laser ablation of the plasma plume

(C) Constant Change of the Plasma

The material expands depending on the vector and recoil of the target surface. The material that is parallel to the vector expands in the plasma hence increasing the background pressure [113]. Consequently, the background pressure of the PLD chamber controls the distribution of the plume. $\cos^n(x)$ law enhances the calculation of the plume density, which depends on the pressure of the chamber. The following stages can be used in explaining the reasons why the shape of the plume expands with pressure.

First and foremost, the splitting or separation of high energetic ions from low energetic ions in the intermediate stage helps in affirming the process. Time of flight data (TOF) can also help in explaining why the shape of the plume depends on the pressure of the background. Secondly, in the vacuum stage, the plume is almost too narrow to cause any scattering concerning the background gases. The plume is forward-directed and narrow; thus, it does not depend much on the background gases. Thirdly, in a high-pressure region, significant diffusion is expected, and the expansion of the material after hitting the target surface. Also, the background gas is vital, and it influences the stoichiometry of the final film that is deposited in the substrate. Therefore, it is imperative to note that increasing the pressure of the background gas can be enhanced by reducing the speed of high energetic ions or species, thus resulting in the expansion of the plasma plume [114].

(D) Ablation Material Deposited

The section is essential in determining the film that is deposited on the substrate in the long run. The material that is ablated hits the substrate surface differently depending on the pressure, and it may lead to damage on the surface and the deposited film. The emitted particles create a region, which eventually creates a source for the condensation of more particles. Then, a high rate of condensation helps in realizing thermal equilibrium, which facilitates the process. The substrate surface is also affected by the ablation materials, which flow into the surface, thus affecting the growth of the film in the long run. The growth of the film depends on the following growth parameters.

Firstly, surface temperature controls the nucleation density, which later affects the deposited film on the substrate. An increase in temperature leads to a decrease in the nucleation density, which is favorable for the deposited film. Carbon (IV) Oxide laser can be used in heating the surface, thus enhancing the decrease of nucleation density. Secondly, the substrate surface where the film is deposited is also vital in determining the quality. The miscut or roughness of the substrate determines the growth of the film, which is deposited. Thirdly, the background pressure and the presence

of gas like oxygen helps in facilitating growth because of the formation of oxides. Low oxygen background will affect the density of nucleation hence leading to low film quality.

Moreover, laser parameters such as laser energy also affect the growth and quality of the film. Pulse laser deposition depends on the nucleation density, which is controlled by laser parameters and supersaturation. Eventually, the parameters officiate the deposition of smooth, quality films on the substrate surface. Therefore, the following growth modes are orchestrated through the laser parameters and other factors highlighted above [115]. Layer by layer growth mode has a goal of coalescence that helps in the generation of large density necessary i8n the growth of films. Islands nucleate more on the surface as more material is added until a perfect density is reached.

Then, the materials continue to grow until they start running into one another hence coalescence. Eventually, when more material is added, they diffuse, and then the process is repeated. Two, there is step flow growth where atoms diffuse before they can go through nucleation. The mode operates best under very high temperatures or high miscut substrate surfaces. The substrates have miscuts associated with the crystal, which leads to the development of atomic steps. Finally, there is the 3D growth mode, which is almost like the previous model only that a new layer is added to the first one. Moreover, the substrate surface becomes rougher since more materials are added.

(E) Deposition rates of films and Influencing Factors

Target material and temperature of the substrate because they control the nucleation density, which affects the film deposited. The pulse energy of the laser and repetition rate of laser affect the target material, thus controlling the rate of deposition. Moreover, the distance from target to substrate affects the movements of the material and how they hit the substrate surface. Most importantly, the type of gas and pressure in the background chamber affects the rate of deposition and quality of the film. For example, oxygen helps in the formation of oxides, which is key to increasing the nucleation density [116].

4.6. MBMT-MAPLE/PLD Technique

The pulsed laser deposition (PLD) is among the most popular applications for laser ablation commonly used in making thin films. In recent years, technology has become very popular due to its unique application in the manufacture of organic coatings. In this paper, a new method used in making nano-composite films will be discussed. Nano-composite films are made through an ablation or evaporation process of multiple organic MAPLE and inorganic PLD targets with several laser beams. One merit of the process is that it resulted in an optimized control and independence of the deposition conditions for different targets. Additionally, the multi-beam and the multi-target deposition systems are included in the discussion. For instance, examples of nano-composite films deposited, and their various properties will be demonstrated as they are encountered and the solutions to the problems that may arise in future trends. The PLD

technique has been over-utilized in the deposition of different kinds of nitrides, oxides, and carbides in the last thirty years. It is also used when thin films are being fabricated, including those that are comprised of semiconductors, electro-optic BaTiO3, and piezoelectric materials, among others [117]. There were many deficiencies in those thin films which were supposed to be addressed before they are made suitable to be applied commercially. Smith and Turner used the technique to prepare the semiconductor and a dielectric film. In their work, they demonstrated stoichiometry transfer between the deposited film and the target. The results showed the deposition rates to be about 0.1nm for every pulse. The target droplets were observed to occur on the surface of the substrate. Even though the results proved to be encouraging to a considerable degree, the PLD technique employed tends to be among the most unsuitable techniques used in making composite films from materials which differ in nature and that are among the reasons why a single laser beam can never be considered enough to be employed in a wide range of materials. A new PLD variant, now known as the concurrent multi-beam multi-target PLD, has seen a further improvement to make it more suitable in a variety of processes. When making nano-composite films a single laser beams among those being used and the target ought to completely suit the process during polymer host deposition like in the case of MAPLE. A polymer solution in a frozen state is used as the laser target in the MAPLE [117]. The solvent concentration and that of the solution are identified based on the polymer's ability to completely dissolve and result in a dilute solution devoid of precipitates. Secondly, the solvent absorbs the laser beam energy; the solute does not. Lastly, there is no hint of a photochemical reaction that is observed when the solute and the solvent react. The interaction between laser radiation and the organic material's matter in the MAPLE is a photothermal process. The conversion of the laser beam energy to thermal energy resulted in heating the polymer, which causes the solvent to vaporize. Also, the polymer molecules get enough kinetic energy as they collide with the solvent molecules as they evaporate as they enter the gas phase. The selection of appropriate MAPLE conditions (laser energy and wavelength, pulse repetition rate, type of solvent, the concentration of polymer solution, temperature, and background gas and its pressure) will result in a deposition process with no significant degradation of the polymer. The MAPLE deposition is carried over layer by layer, while the concentration of the polymer solution remains constant in the ablated target. When a substrate is positioned directly in the path of the plume, the film starts to form, from the evaporated polymer molecules on a substrate placed in the path of the plume. Instantly solvent molecules and particles are removed from the chamber by a vacuum pump, to eliminate any possible contaminations to the forming film. In the case of the fabrication of polymer nanocomposites, MAPLE targets are usually prepared as nano-colloids of additives of interest in the initial polymer solutions. Combining materials of a different nature, such as polymers and inorganic substances, with the same goal and ablating them with the same laser beam, rarely results in fair-quality nano-composite films. The energy and wavelength of the laser beam cannot fit all the components of the mixture. The target dictates the proportion of the components in the film, and it cannot interfere with the process. The concurrent multi-beam multi-target deposition method could be improved through MAPLE polymer targets and in organic PLD targets. All of them should be concurrently ablated through laser beams with varying wavelengths. This technique may also be referred to as a multi-beam target MAPLE and PLD; the acronym for the method is MBMT-MAPLE/PLD.
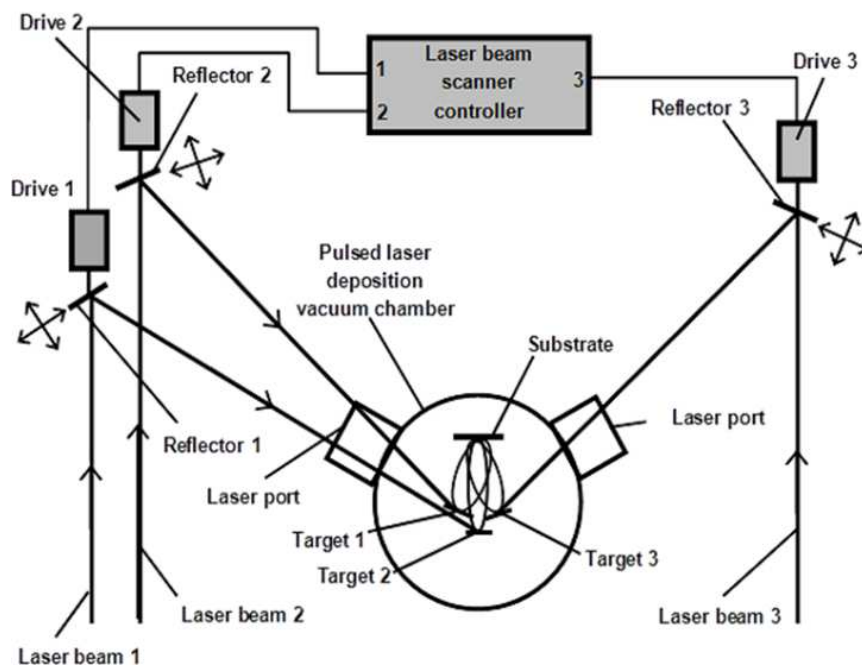

Figure 17. The schematic of the MBMT-MAPLE/PLD system [117].

5. Experimental Details: Simulation and Analysis Approach of Perovskite Solar Cells

Simulation can show the physical operation, the viability of a proposed physical model and is an essential way of understanding the device operation, and how the device parameters affect the physical operation and performance of the solar cell devices instantly without the need to wait for long or spend money prior seen a result. There are various simulation models used throughout the photovoltaics technology (AMPS, COMSOL MULTIPHYSICS, GPVDM, SCAPS, SILVACO, and TCAD). In this paper, we use the SCAPS 1D simulator to model the perovskite-based solar cells [16]; we can define up to 7 semiconductor layers. SCAPS 1D can be used to simulate PSC because it has a very intuitive operation window diversified models for grading, defects, recombination, and generation. Once all parameters defined, it behaves like a real-life counterpart. The following differential equations in one dimension, are applied [16]:

$$\frac{\partial^2}{\partial x^2}\varphi(x) = \frac{q}{\varepsilon}[n(x) - p(x) - N_D^+(x) + N_A^-(x) - p_t(x) + n_t(x)] \quad (2)$$

Poisson's Equation

$$J_{n,p} = nq\mu_n E + qD_n\frac{\partial n}{\partial x} + pq\mu_P E - qD_P\frac{\partial P}{\partial x} \quad (3)$$

Transport equations

$$L_{n,p} = \sqrt{D_{n,p}\tau_{n,p}} \quad (4)$$

Diffusion Length

$$D_{n,p} = [\left(\frac{K_B T}{q}\right)\mu_{n,p} \quad (5)$$

Diffusivity

$$\frac{\partial n,p}{\partial t} = \frac{1}{q}\frac{\partial J_n}{\partial x} + (G_n - R_n) + \frac{1}{q}\frac{\partial J_p}{\partial x} + (G_p - R_p) \quad (6)$$

Continuity equation

$$V_{OC} = \frac{nK_B T}{q}[In\left(\frac{I_L}{I_o} + 1\right)] \quad (7)$$

Where φ: is the electrostatic potential, q is an elementary charge, $\mathcal{E}$ is the permittivity, n is the density of free electron, p is the density of free hole, N_D^+ is the ionized donor (doping density), N_A^- is the ionized acceptor (doping density), p_t is the trapped hole density, n_t is the electron trapped density, Ln,p is the diffusion length of electron and holes, $D_{n,p}$ is the electron, hole Diffusivity, μ_n is the electron mobility, τ_n is the electron lifetime, n,p is the electron/ hole concentration, E is the electric field, $\frac{\partial n,p}{\partial x}$ is the concentration gradient for the electrons/holes, $G_{n,p}$ is the optical generation rate, $R_{n,p}$ is the recombination rate [16], Voc is the open-circuit voltage, n is the ideality factor, $k_B T/q$ is the thermal voltage, I_L is the solar cell light generated current, and I_0 is the reverse saturation current. PSC used in the simulation is an n-i-p structure laid between the n-type semiconductor Titanium Oxide (TiO$_2$) as an Electron Transport Layer (ETL) and p-type Spiro-OMeTAD as a Hole Transport Layer (HTL). A SnO$_2$: F as Fluorine doped Tin Oxide (FTO) is the transparent conductive oxide (TCO), and Au (Gold) as conductor Figure 6 [16]. Solar Cell Capacitance Simulator (SCAPS) is used to simulate PSCs. SCAPS -1D is one of the most widely used device simulators in inorganic solar cells. The simulator uses the three main differential equations 1) Poisson's equation, 2) transport equation, and 3) continuity equation, which is developed by a group of researchers at the University of Gent, Belgium.

5.1. Photovoltaic Characteristics used for Device Modeling

In order to study the PSC, the SCAPS-1D simulator used Figure 18 to show the input panel to start defining the solar cell different layers. Figure 6 shows PSC structure with different layers, such as a contact layer is gold (Au) with a work function of 5.1eV, different contact layers were used, and the work function value and the simulation results are listed in table 1, and table 2, respectively. Also, Spiro-OMeTAD as Hole Transport Layer (HTL), and a p-type with total defect density N$_t$ of 1X10^{15} cm^{-3}. The active layer CH$_3$NH$_3$PBI$_3$ or called the absorber layer, which is the heart of the device [19-20]. It is an n-type material, the density set 9x10^{20}cm^{-3}, and the energetic distribution is Gaussian type, which has a characteristic energy value of 0.1 eV and capture cross-section for the electrons and holes are 2x10^{-14} cm^2 and a defect density of 2.5x10^{13} cm^{-3}, which give a carrier diffusion length for electrons and holes of 1.1µm. The Electron Transport Layer (ETL) is an n-type with total defect density N$_t$ of 1X10^{15} cm^{-3}. The simulations were performed under the Standard Test Condition (STC) AM1.5G, 1000 W/m^2, and T= 300 K.

Table 1. *Photovoltaic characteristics of PSC used in the simulation [16]..*

Characteristics	SnO$_2$: F	TiO$_2$	CH$_3$NH$_3$PBI$_3$	Spiro-OMeTAD
Thickness (nm)	500	100	100-1000	300
bandgap (eV) Eg	3.5	3.2	1.55	2.9
electron affinity (eV) χ	4	4.26	3.9	2.2
dielectric permittivity ϵ_r	9	38-108	30	3
CB effective density of states (1/cm^3)	2.20X10^{17}	2.00X10^{18}	2.20X10^{18}	2.50X10^{18}
VB effective density of states (1/cm^3)	2.20X10^{16}	1.80X10^{19}	1.00X10^{18}	1.80X10^{19}
electron thermal velocity (cm/s)	1X10^7	1X10^7	1X10^7	1X10^7
hole thermal velocity (cm/s)	1X10^7	1X10^7	1X10^7	1X10^7
electron mobility (cm²/Vs)	20	2.X10^4	2.20	2.00X10^{-04}
hole mobility (cm²/Vs)	10	1X10^3	2.2	2.00X10^{-04}

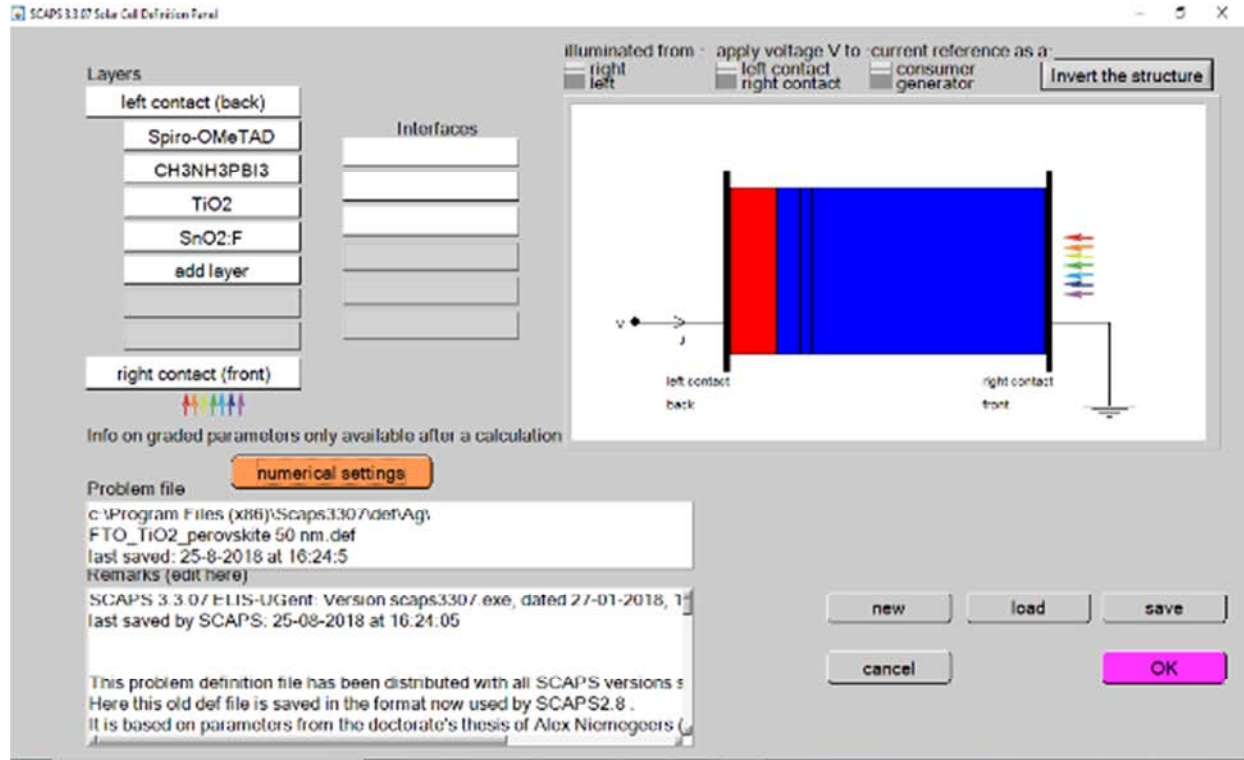| Characteristics	SnO$_2$: F	TiO$_2$	CH$_3$NH$_3$PBI$_3$	Spiro-OMeTAD
shallow uniform donor density ND (1/cm^3)	1X10^{15}	6X10^{19}	9X10^{20}	0
shallow uniform acceptor density NA (1/cm^3)	0	0	0	1X10^{22}
N$_t$ Total (cm^{-3})	1X10^{15}	1X10^{15}	8.50X10^{13}	1X10^{15}
Contacts Au, Ag, Al, Cu, Cr, Pt and Cu-graphite alloy				
Work function (5.1, 4.7, 4.3, 4.65, 4.5, 5.65, 5 eV)				

Figure 18. SCAPS-1D definition panel with PSC cell layers name [16].

Figure 18 shows the SCAPS-1D Solar definition panel as it consists of 7 layers that can be defined with different materials and parameters

5.2. Results and Discussion

In this study, we observed the thickness of the absorber layer, which has a very high absorption coefficient up to 105cm^{-1}. It is a very critical parameter that affects the PSC performance, and it is electrical properties such as (Jsc, Voc, FF, and PCE), the short-circuit current density, the open-circuit voltage, Fill Factor and the power conversion efficiency, respectively. As the absorber thickness (vary from 100 to 1000 nm). The default parameters for the other layers set, as mentioned in Table 1. As shown in Figure 11, which shows the optimal cell performance around the thickness of 500nm for the active layer, and then decreases slightly. While V$_{OC}$ increases to an optimal value at 400nm and then decreases afterward. For fill factor, it increases slowly when the thickness increases. The behavior of the efficiency is very similar to Voc, increasing to an optimal value between 300nm and 500nm, and then decreases with the thickness increase. Also the EQE it decreases as the thickness of the absorber layer increases, which is an indication of electron trapping mechanism, Another critical property is the charge carriers in the perovskite active layer have a longer diffusion length than 500nm as the case of our model, where the electron and hole can reach their corresponding electrode before they recombine, which can enhance the efficiency [16]. Moreover, Voc is defined by equation (8). More excess carrier's concentration gives a higher value of $I L$, while $I 0$ stays at a low level because of not much recombination in the cell. This is the reason why Voc increases for the first time. Fill Factor is defined as the ratio of the maximum generated power to the product of Voc and Isc when the thickness is less than 500nm. However, the PCE is increasing, with the thickness increases to some degree. The internal power depletion is also increasing after 500 nm. While the thickness of more than 500 nm, we start noticing the decreasing effect on the PCE, which caused more recombination to happen because of the increasing number of traps and because more and more excess carriers cannot reach the electrodes. In this case, thicker absorber brings drops of Voc and PCE. In this simulation, the performance of a solar cell is dominated by two factors, 1) How efficient is the active layer can absorb the photon. 2) How fast the charge carrier can move to the corresponding electrode [22-23].

6. Conclusion

We employed the device simulator SCAPS 1D in the

modeling of PSC. SCAPS-1D [24] simulator. The researchers widely use this program from around the world for modeling all types of solar cells. We have used different types of contacts such as Au, Ag, Al, Cu, Cr, Pt, and Cu-graphite alloy

as a contact layer with a work function of 5.1eV, 4.7eV, 4.3eV, 4.65eV, 5.65eV, and 5eV respectively. SPIRO-

OMeTAD, $CH_3NH_3PBI_3$ as an absorber layer with a different thickness between 100nm to 1000nm, the results are shown in Table 2. Figure 11 shows a 500nm thickness is an optimal thickness for the absorber with an efficiency shown in table 2, and TiO_2 as ETL. Also, the EQE decreases as the thickness of the absorber layer increases, which is an indication of electron trapping mechanism.
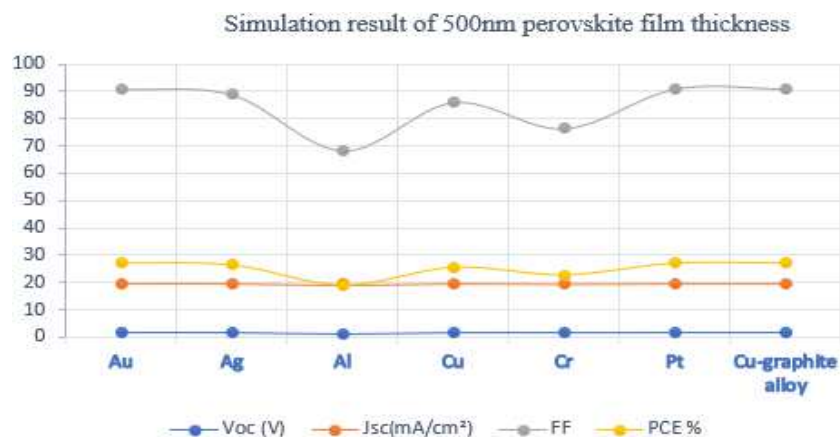
Figure 19. *Shows the simulation results of different contacts material parameters at 500nm thickness of $CH_3NH_3PBI_3$ semiconductor.*

Table 2. *Shows the simulation results.*

Sample at 500nm	Voc (V)	Jsc (mA/cm²)	FF	PCE%
Au	1.51	19.841	90.96	27.25
Ag	1.505	19.841	88.77	26.52
Al	1.396	19.838	68.23	18.9
Cu	1.504	19.841	85.97	25.66
Cr	1.503	19.840	76.33	22.77
Pt	1.51	19.841	90.96	27.25
Cu-graphite alloy	1.51	19.841	90.96	27.25

Acknowledgements

References

[1] K. P. Bhandari and R. J. Ellingson, "An Overview of Hybrid Organic-Inorganic Metal Halide Perovskite Solar Cells," *A Comprehensive Guide to Solar Energy Systems*, pp. 233–254, 2018.

[2] Resources.solarbusinesshub.com, "Global Market Outlook for Solar Power 2016-2020 - Solar Business Hub," *Resources*, Jul-2016. [Online]. Available: https://resources.solarbusinesshub.com/solar-industry-reports/item/global-market-outlook-for-solar-power-2016-2020. [Accessed: 28-Jan-2020].

[3] K. P. Bhandari, J. M. Collier, R. J. Ellingson, and D. S. Apul, "Energy payback time (EPBT) and energy return on energy invested (EROI) of solar photovoltaic systems: A systematic review and meta-analysis," *Renewable and Sustainable Energy Reviews*, vol. 47, pp. 133–141, 2015.

[4] Z. Song, C. L. Mcelvany, A. B. Phillips, I. Celik, P. W. Krantz, S. C. Watthage, G. K. Liyanage, D. Apul, and M. J. Heben, "A techno-economic analysis of perovskite solar module manufacturing with low-cost materials and techniques," *Energy & Environmental Science*, vol. 10, no. 6, pp. 1297–1305, 2017.

[5] S. K. Wallace, D. B. Mitzi, and A. Walsh, "The Steady Rise of Kesterite Solar Cells," *ACS Energy Letters*, vol. 2, no. 4, pp. 776–779, 2017.

[6] W. S. Yang, J. H. Noh, N. J. Jeon, Y. C. Kim, S. Ryu, J. Seo, and S. I. Seok, "High-performance photovoltaic perovskite layers fabricated through intramolecular exchange," *Science*, vol. 348, no. 6240, pp. 1234–1237, 2015.

[7] C.-H. Chiang, M. K. Nazeeruddin, M. Grätzel, and C.-G. Wu, "The synergistic effect of H_2O and DMF towards stable and 20% efficiency inverted perovskite solar cells," *Energy & Environmental Science*, vol. 10, no. 3, pp. 808–817, 2017.

[8] H. Tan, A. Jain, O. Voznyy, X. Lan, F. P. G. D. Arquer, J. Z. Fan, R. Quintero-Bermudez, M. Yuan, B. Zhang, Y. Zhao, F. Fan, P. Li, L. N. Quan, Y. Zhao, Z.-H. Lu, Z. Yang, S. Hoogland, and E. H. Sargent, "Efficient and stable solution-processed planar perovskite solar cells via contact passivation," *Science*, vol. 355, no. 6326, pp. 722–726, 2017.

[9] "Contributed Papers in Specimen Mineralogy: 38th Rochester Mineralogical Symposium: Part 1," *Rocks & Minerals*, vol. 87, no. 2, pp. 171–174, 2012.

[10] D. B. Mitzi, "ChemInform Abstract: Synthesis, Crystal Structure, and Optical and Thermal Properties of $(C_4H_9NH_3)_2MI_4$ (M. Ge, Sn, Pb).," *ChemInform*, vol. 27, no. 26, 2010.

[11] D. B. Mitzi, M. T. Prikas, and K. Chondroudis, "Thin Film Deposition of Organic−Inorganic Hybrid Materials Using a Single Source Thermal Ablation Technique," *Chemistry of Materials*, vol. 11, no. 3, pp. 542–544, 1999.

[12] D. B. Mitzi, C. D. Dimitrakopoulos, and L. L. Kosbar, "Structurally Tailored Organic−Inorganic Perovskites: Optical Properties and Solution-Processed Channel Materials for Thin-Film Transistors," *Chemistry of Materials*, vol. 13, no. 10, pp. 3728–3740, 2001.

[13] K. Chondroudis and D. B. Mitzi, "Electroluminescence from an Organic−Inorganic Perovskite Incorporating a Quaterthiophene Dye within Lead Halide Perovskite Layers," *Chemistry of Materials*, vol. 11, no. 11, pp. 3028–3030, 1999.

[14] J. Ribierre, T. Aoyama, T. Muto, and P. André, "Hybrid organic-inorganic liquid bistable memory devices," *Organic Electronics*, vol. 12, no. 11, pp. 1800–1805, 2011.

[15] D. Wang, M. Wright, N. K. Elumalai, and A. Uddin, "Stability of perovskite solar cells," *Solar Energy Materials and Solar Cells*, vol. 147, pp. 255–275, 2016.

[16] A. Husainat, W. Ali, P. Cofie, J. Attia, and J. Fuller, "Simulation and Analysis of Methylammonium Lead Iodide (CH$_3$NH$_3$PbI$_3$) Perovskite Solar Cell with Au Contact Using SCAPS 1D Simulator," *American Journal of Optics and Photonics*, vol. 7, no. 2, p. 33, 2019.

[17] A. Kojima, K. Teshima, Y. Shirai, and T. Miyasaka, "Organometal Halide Perovskites as Visible-Light Sensitizers for Photovoltaic Cells," *Journal of the American Chemical Society*, vol. 131, no. 17, pp. 6050–6051, 2009.

[18] J.-H. Im, C.-R. Lee, J.-W. Lee, S.-W. Park, and N.-G. Park, "6.5% efficient perovskite quantum-dot-sensitized solar cell," *Nanoscale*, vol. 3, no. 10, p. 4088, 2011.

[19] H.-S. Kim, C.-R. Lee, J.-H. Im, K.-B. Lee, T. Moehl, A. Marchioro, S.-J. Moon, R. Humphry-Baker, J.-H. Yum, J. E. Moser, M. Grätzel, and N.-G. Park, "Lead Iodide Perovskite Sensitized All-Solid-State Submicron Thin Film Mesoscopic Solar Cell with Efficiency Exceeding 9%," *Scientific Reports*, vol. 2, no. 1, 2012.

[20] M. M. Lee, J. Teuscher, T. Miyasaka, T. N. Murakami, and H. J. Snaith, "Efficient Hybrid Solar Cells Based on Meso-Superstructured Organometal Halide Perovskites," *Science*, vol. 338, no. 6107, pp. 643–647, 2012.

[21] "Newcomer Juices Up the Race to Harness Sunlight," *Science*, vol. 342, no. 6165, pp. 1438–1439, 2013.

[22] S. S. Shin, E. J. Yeom, W. S. Yang, S. Hur, M. G. Kim, J. Im, J. Seo, J. H. Noh, and S. I. Seok, "Colloidally prepared La-doped BaSnO 3 electrodes for efficient, photostable perovskite solar cells," *Science*, vol. 356, no. 6334, pp. 167–171, 2017.

[23] A. Ummadisingu, L. Steier, J.-Y. Seo, T. Matsui, A. Abate, W. Tress, and M. Grätzel, "The effect of illumination on the formation of metal halide perovskite films," *Nature*, vol. 545, no. 7653, pp. 208–212, 2017.

[24] J. Burschka, N. Pellet, S.-J. Moon, R. Humphry-Baker, P. Gao, M. K. Nazeeruddin, and M. Grätzel, "Sequential deposition as a route to high-performance perovskite-sensitized solar cells," *Nature*, vol. 499, no. 7458, pp. 316–319, 2013.

[25] D. Liu and T. L. Kelly, "Perovskite solar cells with a planar heterojunction structure prepared using room-temperature solution processing techniques," *Nature Photonics*, vol. 8, no. 2, pp. 133–138, 2013.

[26] Q. Chen, H. Zhou, Z. Hong, S. Luo, H.-S. Duan, H.-H. Wang, Y. Liu, G. Li, and Y. Yang, "Planar Heterojunction Perovskite Solar Cells via Vapor-Assisted Solution Process," *Journal of the American Chemical Society*, vol. 136, no. 2, pp. 622–625, 2013.

[27] M. Liu, M. B. Johnston, and H. J. Snaith, "Efficient planar heterojunction perovskite solar cells by vapour deposition," *Nature*, vol. 501, no. 7467, pp. 395–398, 2013.

[28] C.-W. Chen, H.-W. Kang, S.-Y. Hsiao, P.-F. Yang, K.-M. Chiang, and H.-W. Lin, "Efficient and Uniform Planar-Type Perovskite Solar Cells by Simple Sequential Vacuum Deposition," *Advanced Materials*, vol. 26, no. 38, pp. 6647–6652, 2014.

[29] W.-J. Yin, T. Shi, and Y. Yan, "Unique Properties of Halide Perovskites as Possible Origins of the Superior Solar Cell Performance," *Advanced Materials*, vol. 26, no. 27, pp. 4653–4658, 2014.

[30] M. Solomon and A. Johnson, "New Research in Solar Cells: Urbach Tails and Open Circuit Voltage," *Elements*, vol. 11, no. 1, 2015.

[31] S. D. Wolf, J. Holovsky, S.-J. Moon, P. Löper, B. Niesen, M. Ledinsky, F.-J. Haug, J.-H. Yum, and C. Ballif, "Organometallic Halide Perovskites: Sharp Optical Absorption Edge and Its Relation to Photovoltaic Performance," *The Journal of Physical Chemistry Letters*, vol. 5, no. 6, pp. 1035–1039, 2014.

[32] G. E. Eperon, S. D. Stranks, C. Menelaou, M. B. Johnston, L. M. Herz, and H. J. Snaith, "Formamidinium lead trihalide: a broadly tunable perovskite for efficient planar heterojunction solar cells," *Energy & Environmental Science*, vol. 7, no. 3, p. 982, 2014.

[33] Y. Li, B. Ding, Q.-Q. Chu, G.-J. Yang, M. Wang, C.-X. Li, and C.-J. Li, "Ultra-high open-circuit voltage of perovskite solar cells induced by nucleation thermodynamics on rough substrates," *Scientific Reports*, vol. 7, no. 1, 2017.

[34] W. Tress, N. Marinova, O. Inganäs, M. K. Nazeeruddin, S. M. Zakeeruddin, and M. Graetzel, "Predicting the Open-Circuit Voltage of CH$_3$NH$_3$PbI$_3$ Perovskite Solar Cells Using Electroluminescence and Photovoltaic Quantum Efficiency Spectra: the Role of Radiative and Non-Radiative Recombination," *Advanced Energy Materials*, vol. 5, no. 3, p. 1400812, 2014.

[35] C. Wehrenfennig, G. E. Eperon, M. B. Johnston, H. J. Snaith, and L. M. Herz, "High Charge Carrier Mobilities and Lifetimes in Organolead Trihalide Perovskites," *Advanced Materials*, vol. 26, no. 10, pp. 1584–1589, 2013.

[36] T. Leijtens, S. D. Stranks, G. E. Eperon, R. Lindblad, E. M. J. Johansson, I. J. Mcpherson, H. Rensmo, J. M. Ball, M. M. Lee, and H. J. Snaith, "Electronic Properties of Meso-Superstructure and Planar Organometal Halide Perovskite Films: Charge Trapping, Photodoping, and Carrier Mobility," *ACS Nano*, vol. 8, no. 7, pp. 7147–7155, 2014.

[37] D. Shi, V. Adinolfi, R. Comin, M. Yuan, E. Alarousu, A. Buin, Y. Chen, S. Hoogland, A. Rothenberger, K. Katsiev, Y. Losovyj, X. Zhang, P. A. Dowben, O. F. Mohammed, E. H. Sargent, and O. M. Bakr, "Low trap-state density and long carrier diffusion in organolead trihalide perovskite single crystals," *Science*, vol. 347, no. 6221, pp. 519–522, 2015.

[38] D. Kiermasch, P. Rieder, K. Tvingstedt, A. Baumann, and V. Dyakonov, "Improved charge carrier lifetime in planar perovskite solar cells by bromine doping," *Scientific Reports*, vol. 6, no. 1, 2016.

[39] S. D. Stranks, G. E. Eperon, G. Grancini, C. Menelaou, M. J. P. Alcocer, T. Leijtens, L. M. Herz, A. Petrozza, and H. J. Snaith, "Electron-Hole Diffusion Lengths Exceeding 1 Micrometer in an Organometal Trihalide Perovskite Absorber," *Science*, vol. 342, no. 6156, pp. 341–344, 2013.

[40] Y. Chen, H. T. Yi, X. Wu, R. Haroldson, Y. N. Gartstein, Y. I. Rodionov, K. S. Tikhonov, A. Zakhidov, X.-Y. Zhu, and V. Podzorov, "Extended carrier lifetimes and diffusion in hybrid perovskites revealed by Hall effect and photoconductivity measurements," *Nature Communications*, vol. 7, no. 1, 2016.

[41] F. D. Angelis, "Origin of high open-circuit voltage in lead-halide perovskite solar cells," *Proceedings of the 10th International Conference on Hybrid and Organic Photovoltaics*, 2018.

[42] T. Baikie, Y. Fang, J. M. Kadro, M. Schreyer, F. Wei, S. G. Mhaisalkar, M. Graetzel, and T. J. White, "Synthesis and crystal chemistry of the hybrid perovskite $(CH_3NH_3)PbI_3$ for solid-state sensitized solar cell applications," *Journal of Materials Chemistry A*, vol. 1, no. 18, p. 5628, 2013.

[43] "Synthesis, Properties, and Crystal Chemistry of Perovskite-Based Materials," 2006.

[44] N. J. Jeon, H. G. Lee, Y. C. Kim, J. Seo, J. H. Noh, J. Lee, and S. I. Seok, "o-Methoxy Substituents in Spiro-OMeTAD for Efficient Inorganic–Organic Hybrid Perovskite Solar Cells," *Journal of the American Chemical Society*, vol. 136, no. 22, pp. 7837–7840, 2014.

[45] J. You, Y. (M. Yang, Z. Hong, T.-B. Song, L. Meng, Y. Liu, C. Jiang, H. Zhou, W.-H. Chang, G. Li, and Y. Yang, "Moisture assisted perovskite film growth for high-performance solar cells," *Applied Physics Letters*, vol. 105, no. 18, p. 183902, 2014.

[46] H. Fu, "Review of lead-free halide perovskites as light-absorbers for photovoltaic applications: From materials to solar cells," *Solar Energy Materials and Solar Cells*, vol. 193, pp. 107–132, 2019.

[47] A. Walsh and G. W. Watson, "The origin of the stereochemically active Pb(II) lone pair: DFT calculations on PbO and PbS," *Journal of Solid State Chemistry*, vol. 178, no. 5, pp. 1422–1428, 2005.

[48] A. Walsh, D. J. Payne, R. G. Egdell, and G. W. Watson, "Stereochemistry of post-transition metal oxides: revision of the classical lone pair model," *Chemical Society Reviews*, vol. 40, no. 9, p. 4455, 2011.

[49] K. T. Butler, J. M. Frost, and A. Walsh, "Band alignment of the hybrid halide perovskites $CH_3NH_3PbCl_3$, $CH_3NH_3PbBr_3$ and $CH_3NH_3PbI_3$," *Materials Horizons*, vol. 2, no. 2, pp. 228–231, 2015.

[50] F. Mandl, "American Institute of Physics Handbook 3rd end," *Physics Bulletin*, vol. 24, no. 8, pp. 492–492, 1973.

[51] C. Grätzel and S. M. Zakeeruddin, "Recent trends in mesoscopic solar cells based on molecular and nano pigments light harvesters," *Materials Today*, vol. 16, no. 1-2, pp. 11–18, 2013.

[52] J. J. Choi, X. Yang, Z. M. Norman, S. J. L. Billinge, and J. S. Owen, "Structure of Methylammonium Lead Iodide Within Mesoporous Titanium Dioxide: Active Material in High-Performance Perovskite Solar Cells," *Nano Letters*, vol. 14, no. 1, pp. 127–133, 2013.

[53] T. Leijtens, G. E. Eperon, S. Pathak, A. Abate, M. M. Lee, and H. J. Snaith, "Overcoming ultraviolet light instability of sensitized TiO_2 with meso-superstructured organometal trihalide perovskite solar cells," *Nature Communications*, vol. 4, no. 1, 2013.

[54] D. Bi, C. Yi, J. Luo, J.-D. Décoppet, F. Zhang, S. M. Zakeeruddin, X. Li, A. Hagfeldt, and M. Grätzel, "Polymer-templated nucleation and crystal growth of perovskite films for solar cells with efficiency greater than 21%," *Nature Energy*, vol. 1, no. 10, 2016.

[55] J.-Y. Jeng, Y.-F. Chiang, M.-H. Lee, S.-R. Peng, T.-F. Guo, P. Chen, and T.-C. Wen, "$CH_3NH_3PbI_3$ Perovskite/Fullerene Planar-Heterojunction Hybrid Solar Cells," *Advanced Materials*, vol. 25, no. 27, pp. 3727–3732, 2013.

[56] J. Y. Jeng, K.-C. Chen, T.-Y. Chiang, P.-Y. Lin, T.-D. Tsai, Y.-C. Chang, T.-F. Guo, P. Chen, T.-C. Wen, and Y.-J. Hsu, "Nickel Oxide Electrode Interlayer in $CH_3NH_3PbI_3$ Perovskite/PCBM Planar-Heterojunction Hybrid Solar Cells," *Advanced Materials*, vol. 26, no. 24, pp. 4107–4113, 2014.

[57] H. Li, W. Shi, W. Huang, E.-P. Yao, J. Han, Z. Chen, S. Liu, Y. Shen, M. Wang, and Y. Yang, "Carbon Quantum Dots/TiOx Electron Transport Layer Boosts Efficiency of Planar Heterojunction Perovskite Solar Cells to 19%," *Nano Letters*, vol. 17, no. 4, pp. 2328–2335, 2017.

[58] J. H. Heo, H. J. Han, D. Kim, T. K. Ahn, and S. H. Im, "Hysteresis-less inverted $CH_3NH_3PbI_3$ planar perovskite hybrid solar cells with 18.1% power conversion efficiency," *Energy & Environmental Science*, vol. 8, no. 5, pp. 1602–1608, 2015.

[59] C. Bi, Q. Wang, Y. Shao, Y. Yuan, Z. Xiao, and J. Huang, "Non-wetting surface-driven high-aspect-ratio crystalline grain growth for efficient hybrid perovskite solar cells," *Nature Communications*, vol. 6, no. 1, 2015.

[60] Q. Dong, Y. Yuan, Y. Shao, Y. Fang, Q. Wang, and J. Huang, "Abnormal crystal growth in $CH_3NH_3PbI_3−xClx$ using a multi-cycle solution coating process," *Energy & Environmental Science*, vol. 8, no. 8, pp. 2464–2470, 2015.

[61] W. Nie, H. Tsai, R. Asadpour, J.-C. Blancon, A. J. Neukirch, G. Gupta, J. J. Crochet, M. Chhowalla, S. Tretiak, M. A. Alam, H.-L. Wang, and A. D. Mohite, "High-efficiency solution-processed perovskite solar cells with millimeter-scale grains," *Science*, vol. 347, no. 6221, pp. 522–525, 2015.

[62] J. You, L. Meng, T.-B. Song, T.-F. Guo, Y. (M. Yang, W.-H. Chang, Z. Hong, H. Chen, H. Zhou, Q. Chen, Y. Liu, N. D. Marco, and Y. Yang, "Improved air stability of perovskite solar cells via solution-processed metal oxide transport layers," *Nature Nanotechnology*, vol. 11, no. 1, pp. 75–81, 2015.

[63] P.-W. Liang, C.-C. Chueh, S. T. Williams, and A. K.-Y. Jen, "Roles of Fullerene-Based Interlayers in Enhancing the Performance of Organometal Perovskite Thin-Film Solar Cells," *Advanced Energy Materials*, vol. 5, no. 10, p. 1402321, 2015.

[64] J. H. Park, J. Seo, S. Park, S. S. Shin, Y. C. Kim, N. J. Jeon, H.-W. Shin, T. K. Ahn, J. H. Noh, S. C. Yoon, C. S. Hwang, and S. I. Seok, "Efficient $CH_3NH_3PbI_3$ Perovskite Solar Cells Employing Nanostructured p-Type NiO Electrode Formed by a Pulsed Laser Deposition," *Advanced Materials*, vol. 27, no. 27, pp. 4013–4019, 2015.

[65] Y. Rong, Z. Tang, Y. Zhao, X. Zhong, S. Venkatesan, H. Graham, M. Patton, Y. Jing, A. M. Guloy, and Y. Yao, "Solvent engineering towards controlled grain growth in perovskite planar heterojunction solar cells," *Nanoscale*, vol. 7, no. 24, pp. 10595–10599, 2015.

[66] H. Tanaka, Y. Ohishi, and T. Oku, "Effects of hot airflow during spin-coating process on CH₃NH₃PbI₃-xClx perovskite solar cells," 2018.

[67] H. Chen, Z. Wei, H. He, X. Zheng, K. S. Wong, and S. Yang, "Solvent Engineering Boosts the Efficiency of Paintable Carbon-Based Perovskite Solar Cells to Beyond 14%," *Advanced Energy Materials*, vol. 6, no. 8, p. 1502087, 2016.

[68] W. Li, J. Fan, J. Li, Y. Mai, and L. Wang, "Controllable Grain Morphology of Perovskite Absorber Film by Molecular Self-Assembly toward Efficient Solar Cell Exceeding 17%," *Journal of the American Chemical Society*, vol. 137, no. 32, pp. 10399–10405, 2015.

[69] H.-B. Kim, H. Choi, J. Jeong, S. Kim, B. Walker, S. Song, and J. Y. Kim, "Mixed solvents for the optimization of morphology in solution-processed, inverted-type perovskite/fullerene hybrid solar cells," *Nanoscale*, vol. 6, no. 12, p. 6679, 2014.

[70] N. Sakai, S. Pathak, H.-W. Chen, A. A. Haghighirad, S. D. Stranks, T. Miyasaka, and H. J. Snaith, "The mechanism of toluene-assisted crystallization of organic–inorganic perovskites for highly efficient solar cells," *Journal of Materials Chemistry A*, vol. 4, no. 12, pp. 4464–4471, 2016.

[71] M. Xiao, F. Huang, W. Huang, Y. Dkhissi, Y. Zhu, J. Etheridge, A. Gray-Weale, U. Bach, Y.-B. Cheng, and L. Spiccia, "A Fast Deposition-Crystallization Procedure for Highly Efficient Lead Iodide Perovskite Thin-Film Solar Cells," *Angewandte Chemie International Edition*, vol. 53, no. 37, pp. 9898–9903, 2014.

[72] Y. Zhou, M. Yang, W. Wu, A. L. Vasiliev, K. Zhu, and N. P. Padture, "Room-temperature crystallization of hybrid-perovskite thin films via solvent–solvent extraction for high-performance solar cells," *Journal of Materials Chemistry A*, vol. 3, no. 15, pp. 8178–8184, 2015.

[73] P. You and F. Yan, "Organic-Inorganic Hybrid Perovskites for Solar Energy Conversion," *Ferroelectric Materials for Energy Applications*, pp. 95–117, 2018.

[74] N. R. Poespawati, I. Dzikri, J. Sulistianto, T. Abuzairi, M. Hariadi, and R. W. Purnamaningsih, "Perovskite Solar Cells Based on Organic-metal halide Perovskite Materials," *2018 4th International Conference on Nano Electronics Research and Education (ICNERE)*, 2018.

[75] D. W. D. Quilettes, S. M. Vorpahl, S. D. Stranks, H. Nagaoka, G. E. Eperon, M. E. Ziffer, H. J. Snaith, and D. S. Ginger, "Impact of microstructure on local carrier lifetime in perovskite solar cells," *Science*, vol. 348, no. 6235, pp. 683–686, 2015.

[76] B. S. Tosun and H. W. Hillhouse, "Enhanced Carrier Lifetimes of Pure Iodide Hybrid Perovskite via Vapor-Equilibrated Re-Growth (VERG)," *The Journal of Physical Chemistry Letters*, vol. 6, no. 13, pp. 2503–2508, 2015.

[77] Z. Xiao, Q. Dong, C. Bi, Y. Shao, Y. Yuan, and J. Huang, "Solvent Annealing of Perovskite-Induced Crystal Growth for Photovoltaic-Device Efficiency Enhancement," *Advanced Materials*, vol. 26, no. 37, pp. 6503–6509, 2014.

[78] J. Troughton, C. Charbonneau, M. J. Carnie, M. L. Davies, D. A. Worsley, and T. M. Watson, "Rapid processing of perovskite solar cells in under 2.5 seconds," *Journal of Materials Chemistry A*, vol. 3, no. 17, pp. 9123–9127, 2015.

[79] J. Troughton, M. J. Carnie, M. L. Davies, C. Charbonneau, E. H. Jewell, D. A. Worsley, and T. M. Watson, "Photonic flash-annealing of lead halide perovskite solar cells in 1 ms," *Journal of Materials Chemistry A*, vol. 4, no. 9, pp. 3471–3476, 2016.

[80] B. W. Lavery, S. Kumari, H. Konermann, G. L. Draper, J. Spurgeon, and T. Druffel, "Intense Pulsed Light Sintering of CH₃NH₃PbI₃ Solar Cells," *ACS Applied Materials & Interfaces*, vol. 8, no. 13, pp. 8419–8426, 2016.

[81] M. Saliba, K. W. Tan, H. Sai, D. T. Moore, T. Scott, W. Zhang, L. A. Estroff, U. Wiesner, and H. J. Snaith, "Influence of Thermal Processing Protocol upon the Crystallization and Photovoltaic Performance of Organic–Inorganic Lead Trihalide Perovskites," *The Journal of Physical Chemistry C*, vol. 118, no. 30, pp. 17171–17177, 2014.

[82] J. H. Noh, S. H. Im, J. H. Heo, T. N. Mandal, and S. I. Seok, "Chemical Management for Colorful, Efficient, and Stable Inorganic–Organic Hybrid Nanostructured Solar Cells," *Nano Letters*, vol. 13, no. 4, pp. 1764–1769, 2013.

[83] T. M. Koh, K. Fu, Y. Fang, S. Chen, T. C. Sum, N. Mathews, S. G. Mhaisalkar, P. P. Boix, and T. Baikie, "Formamidinium-Containing Metal-Halide: An Alternative Material for Near-IR Absorption Perovskite Solar Cells," *The Journal of Physical Chemistry C*, vol. 118, no. 30, pp. 16458–16462, 2013.

[84] C. C. Stoumpos, C. D. Malliakas, and M. G. Kanatzidis, "Semiconducting Tin and Lead Iodide Perovskites with Organic Cations: Phase Transitions, High Mobilities, and Near-Infrared Photoluminescent Properties," *Inorganic Chemistry*, vol. 52, no. 15, pp. 9019–9038, 2013.

[85] N. Pellet, P. Gao, G. Gregori, T.-Y. Yang, M. K. Nazeeruddin, J. Maier, and M. Grätzel, "Mixed-Organic-Cation Perovskite Photovoltaics for Enhanced Solar-Light Harvesting," *Angewandte Chemie*, vol. 126, no. 12, pp. 3215–3221, 2014.

[86] S. Gubbala, V. Chakrapani, V. Kumar, and M. K. Sunkara, "Band-Edge Engineered Hybrid Structures for Dye-Sensitized Solar Cells Based on SnO₂ Nanowires," *Advanced Functional Materials*, vol. 18, no. 16, pp. 2411–2418, 2008.

[87] D.-Y. Son, J.-H. Im, H.-S. Kim, and N.-G. Park, "11% Efficient Perovskite Solar Cell Based on ZnO Nanorods: An Effective Charge Collection System," *The Journal of Physical Chemistry C*, vol. 118, no. 30, pp. 16567–16573, 2014.

[88] R. Zhang, C. Fei, B. Li, H. Fu, J. Tian, and G. Cao, "Continuous Size Tuning of Monodispersed ZnO Nanoparticles and Its Size Effect on the Performance of Perovskite Solar Cells," *ACS Applied Materials & Interfaces*, vol. 9, no. 11, pp. 9785–9794, 2017.

[89] J. Yun, J. Ryu, J. Lee, H. Yu, and J. Jang, "SiO₂/TiO₂ based hollow nanostructures as scaffold layers and Al-doping in the electron transfer layer for efficient perovskite solar cells," *Journal of Materials Chemistry A*, vol. 4, no. 4, pp. 1306–1311, 2016.

[90] A. Mei, X. Li, L. Liu, Z. Ku, T. Liu, Y. Rong, M. Xu, M. Hu, J. Chen, Y. Yang, M. Gratzel, and H. Han, "A hole-conductor-free, fully printable mesoscopic perovskite solar cell with high stability," *Science*, vol. 345, no. 6194, pp. 295–298, 2014.

[91] S. G. Hashmi, D. Martineau, X. Li, M. Ozkan, A. Tiihonen, M. I. Dar, T. Sarikka, S. M. Zakeeruddin, J. Paltakari, P. D. Lund, and M. Grätzel, "Air Processed Inkjet Infiltrated Carbon Based Printed Perovskite Solar Cells with High Stability and Reproducibility," *Advanced Materials Technologies*, vol. 2, no. 1, p. 1600183, 2016.

[92] A. Bera, K. Wu, A. Sheikh, E. Alarousu, O. F. Mohammed, and T. Wu, "Perovskite Oxide $SrTiO_3$ as an Efficient Electron Transporter for Hybrid Perovskite Solar Cells," *The Journal of Physical Chemistry C*, vol. 118, no. 49, pp. 28494–28501, 2014.

[93] J. P. C. Baena, L. Steier, W. Tress, M. Saliba, S. Neutzner, T. Matsui, F. Giordano, T. J. Jacobsson, A. R. S. Kandada, S. M. Zakeeruddin, A. Petrozza, A. Abate, M. K. Nazeeruddin, M. Grätzel, and A. Hagfeldt, "Highly efficient planar perovskite solar cells through band alignment engineering," *Energy & Environmental Science*, vol. 8, no. 10, pp. 2928–2934, 2015.

[94] J. Liu, C. Gao, L. Luo, Q. Ye, X. He, L. Ouyang, X. Guo, D. Zhuang, C. Liao, J. Mei, and W. Lau, "Low-temperature, solution processed metal sulfide as an electron transport layer for efficient planar perovskite solar cells," *Journal of Materials Chemistry A*, vol. 3, no. 22, pp. 11750–11755, 2015.

[95] L. Wang, W. Fu, Z. Gu, C. Fan, X. Yang, H. Li, and H. Chen, "Low temperature solution processed planar heterojunction perovskite solar cells with a CdSe nanocrystal as an electron transport/extraction layer," *J. Mater. Chem. C*, vol. 2, no. 43, pp. 9087–9090, 2014.

[96] J. T.-W. Wang, J. M. Ball, E. M. Barea, A. Abate, J. A. Alexander-Webber, J. Huang, M. Saliba, I. Mora-Sero, J. Bisquert, H. J. Snaith, and R. J. Nicholas, "Low-Temperature Processed Electron Collection Layers of Graphene/TiO_2 Nanocomposites in Thin Film Perovskite Solar Cells," *Nano Letters*, vol. 14, no. 2, pp. 724–730, 2013.

[97] C.-H. Chiang, Z.-L. Tseng, and C.-G. Wu, "Planar heterojunction perovskite/PC71BM solar cells with enhanced open-circuit voltage via a (2/1)-step spin-coating process," *J. Mater. Chem. A*, vol. 2, no. 38, pp. 15897–15903, 2014.

[98] P. Docampo, J. M. Ball, M. Darwich, G. E. Eperon, and H. J. Snaith, "Efficient organometal trihalide perovskite planar-heterojunction solar cells on flexible polymer substrates," *Nature Communications*, vol. 4, no. 1, 2013.

[99] G. Xing, N. Mathews, S. Sun, S. S. Lim, Y. M. Lam, M. Gratzel, S. Mhaisalkar, and T. C. Sum, "Long-Range Balanced Electron- and Hole-Transport Lengths in Organic-Inorganic $CH_3NH_3PbI_3$," *Science*, vol. 342, no. 6156, pp. 344–347, 2013.

[100] G. E. Eperon, V. M. Burlakov, P. Docampo, A. Goriely, and H. J. Snaith, "Morphological Control for High Performance, Solution-Processed Planar Heterojunction Perovskite Solar Cells," *Advanced Functional Materials*, vol. 24, no. 1, pp. 151–157, 2013.

[101] R. Liu and K. Xu, "Solvent Engineering for Perovskite solar cells: A Review," *Micro & Nano Letters*, 2020.

[102] J. M. Ball, M. M. Lee, A. Hey, and H. J. Snaith, "Low-temperature processed meso-superstructured to thin-film perovskite solar cells," *Energy & Environmental Science*, vol. 6, no. 6, p. 1739, 2013.

[103] J. You, Z. Hong, Y. (M. Yang, Q. Chen, M. Cai, T.-B. Song, C.-C. Chen, S. Lu, Y. Liu, H. Zhou, and Y. Yang, "Low-Temperature Solution-Processed Perovskite Solar Cells with High Efficiency and Flexibility," *ACS Nano*, vol. 8, no. 2, pp. 1674–1680, 2014.

[104] Z. Song, S. C. Watthage, A. B. Phillips, and M. J. Heben, "Pathways toward high-performance perovskite solar cells: review of recent advances in organo-metal halide perovskites for photovoltaic applications," *Journal of Photonics for Energy*, vol. 6, no. 2, p. 022001, 2016.

[105] Y. Yu, C. Wang, C. R. Grice, N. Shrestha, J. Chen, D. Zhao, W. Liao, A. J. Cimaroli, P. J. Roland, R. J. Ellingson, and Y. Yan, "Improving the Performance of Formamidinium and Cesium Lead Triiodide Perovskite Solar Cells using Lead Thiocyanate Additives," *ChemSusChem*, vol. 9, no. 23, pp. 3288–3297, 2016.

[106] C. Roldán-Carmona, P. Gratia, I. Zimmermann, G. Grancini, P. Gao, M. Graetzel, and M. K. Nazeeruddin, "High efficiency methylammonium lead triiodide perovskite solar cells: the relevance of non-stoichiometric precursors," *Energy & Environmental Science*, vol. 8, no. 12, pp. 3550–3556, 2015.

[107] Q. Meng, "Energy and interface engineering for perovskite solar cells," *International Photonics and OptoElectronics*, 2015.

[108] Z. Song, S. C. Watthage, A. B. Phillips, B. L. Tompkins, R. J. Ellingson, and M. J. Heben, "Impact of Processing Temperature and Composition on the Formation of Methylammonium Lead Iodide Perovskites," *Chemistry of Materials*, vol. 27, no. 13, pp. 4612–4619, 2015.

[109] Q. Wang, Y. Shao, Q. Dong, Z. Xiao, Y. Yuan, and J. Huang, "Large fill-factor bilayer iodine perovskite solar cells fabricated by a low-temperature solution-process," *Energy Environ. Sci.*, vol. 7, no. 7, pp. 2359–2365, 2014.

[110] J.-H. Im, I.-H. Jang, N. Pellet, M. Grätzel, and N.-G. Park, "Growth of $CH_3NH_3PbI_3$ cuboids with controlled size for high-efficiency perovskite solar cells," *Nature Nanotechnology*, vol. 9, no. 11, pp. 927–932, 2014.

[111] M. Golitko and L. Dussubieux, "Inductively Coupled Plasma-Mass Spectrometry (ICP-MS) and Laser Ablation Inductively Coupled Plasma-Mass Spectrometry (LA-ICP-MS)," *The Oxford Handbook of Archaeological Ceramic Analysis*, pp. 398–423, 2016.

[112] S. Neralla, S. Yarmolenko, D. Kumar, D. Pai, and J. Sankar, "Cross-Sectional Nanoindentation of Alumina Thin Films Deposited by Pulsed Laser Deposition Process," *Materials, Nondestructive Evaluation, and Pressure Vessels and Piping*, 2006.

[113] A. Sivkov, E. Naiden, A. Ivashutenko, and I. Shanenkov, "Plasma dynamic synthesis and obtaining ultrafine powders of iron oxides with high content of ε-Fe_2O_3," *Journal of Magnetism and Magnetic Materials*, vol. 405, pp. 158–168, 2016.

[114] M. H. Azhdast, G. Azdasht, H. Lüdeke, K.-D. Lang, and V. Glaw, "Nano particle production by laser ablation and metal sputtering on Si-Wafer substrate," *Advanced Solid State Lasers*, 2015.

[115] N. K. Ponon, D. J. Appleby, E. Arac, P. King, S. Ganti, K. S. Kwa, and A. O'neill, "Effect of deposition conditions and post deposition anneal on reactively sputtered titanium nitride thin films," *Thin Solid Films*, vol. 578, pp. 31–37, 2015.

[116] Inc, "Pulsed Laser Deposition Systems - PVD Products," *Pulsed Laser Deposition Systems - PVD Products*. [Online]. Available: Http://www.pvdproducts.com/pulsed-laser-deposition-systems. [Accessed: 28-Jan-2020].

[117] A. M. Darwish, S. S. Sarkisov, and D. N. Patel, "Concurrent Multi-Target Laser Ablation for Making Nano-Composite Films," *Applications of Laser Ablation - Thin Film Deposition, Nanomaterial Synthesis and Surface Modification*, 2016.

[118] K. Wojciechowski, M. Saliba, T. Leijtens, A. Abate, and H. J. Snaith, "Sub-150 °C processed meso-superstructured perovskite solar cells with enhanced efficiency," *Energy Environ. Sci.*, vol. 7, no. 3, pp. 1142–1147, 2014.

[119] C. Aranda, J. Bisquert, and A. Guerrero, "High open – circuit voltatge of pure bromide perovskite solar cells using spiro-ometad as a hole-selective material," *Proceedings of the 3rd International Conference on Perovskite Thin Film Photovoltaics, Photonics and Optoelectronics*, 2017.

[120] "Pulsed laser deposition," *Wikipedia*, 14-Dec-2019. [Online]. Available: https://en.wikipedia.org/wiki/Pulsed_laser_deposition. [Accessed: 29-Jan-2020].